Hydrodynamics of Jet-driven Liquid-liquid Inverse Droplet Flow and Its Application for Separation of Organic Contaminants

THESIS

Submitted in Partial Fulfillment of the

Requirements for the Degree of

Doctor of Philosophy

In

Engineering

By

Bongliba T Sangtam

Roll No.: 176107032

Under the Supervision of

Prof. Subarata Kumar Majumder

DEPARTMENT OF CHEMICAL ENGINEERING

INDIAN INSTITUTE OF TCHNOLOGY GUWAHATI

GUWAHATI – 781039, INDIA

Dedicated

to

My Parents and Siblings

DEPARTMENT OF CHEMICAL ENGINEERING

INDIAN INSTITUTE OF TECHNOLOGY GUWAHATI

GUWAHATI – 781039, INDIA

DEPARTMENT OF CHEMICAL ENGINEERING

CERTIFICATE

This is to certify that the thesis entitled "**Hydrodynamics of Jet-driven Liquid-liquid Inverse Droplet Flow and Its Application for Separation of Organic Contaminants"** submitted by **Mr. Bongliba T Sangtam** in fulfillment of the requirement of the Degree of Doctor of Philosophy in Engineering is a record of bonafide research work carried out by him, in the Department of Chemical Engineering, Indian Institute of Technology Guwahati, under my guidance and supervision. The work documented in this thesis has not been submitted to any other University or Institute for the award of any degree or diploma. In my opinion, the thesis has met the standard for fulfilling the requirements of the Ph.D. degree as prescribed in the regulations of this institute

Prof. Subarata Kumar Majumder

Professor

Department of Chemical Engineering

Indian Institute of Technology Guwahati

Guwahati – 781039, Assam, India

ACKNOWLEDGEMENTS

I would like to express my special appreciation and gratitude to my beloved supervisor **Prof. Subarata Kumar Majumder** for putting a tremendous amount of effort, enthusiasm, support, and dedication towards my research. His philosophical guidance has built up momentum inside me, and I will carry his energy and positive attitude with me in my future endeavors. His commitment approach towards my experimental works, data analysis, writing manuscripts, and thesis within the stipulated time helped me to complete my research work. Whenever I felt discouraged in my personal life or in academic, my professor used to cheer me with words of encouragement, which enabled me to stay on track during throughout my research journey.

I would also like to thank **Prof. Anugrah Singh**, Head of Department, Department of Chemical Engineering for providing research facilities in the department. I am also grateful to all of the faculty members in the department for their assistance and support. I must also thank my doctoral committee members **Dr. Venkates R. Prasanna**, **Dr. Vairakannu Prabu** in the Department of Chemical Engineering, and **Dr. Anil Kumar Mishra** in the Department of Civil Engineering, for their valuable suggestions and contribution towards my research work.

I would like to thank **Dr. Kaustavmoni Deka**, Technical Superintendent in the Department of Chemical Engineering, for his constant help whenever I have questions relating to chemistry for my works. I also would like to thank the other non-teaching staff for their corporation. I also would like to express my gratitude to my labmates, **Dr. Ritesh Prakash**, **Dr. Goshika Kumar Bharat**, **Mr. Kalichran Hembrom**, **Dr. Fahad M K**, **Dr. Somen Mondal**, **Ms. Surabhi Patel**, **Miss. Stuti Dubey**, **Mr. Mohd Tauhid Khan**, **Ms. Kumari Rubey**, **Mr. Jinesh Machale**, **Mr. Yogesh Gupta**, **Mr. Gourav Singh**, **Mr. Kashis Dhir**, **Mr. Kumar Kartikey Singh**, **Mr. Ashutosh Singh**, **Mr. Pathari Yash Subash**, **Ms. V V R S Bhavana**, and **Mr. Babban Lal Maurya** for their company and support during my research work. Especially, I would like to extend my gratitude to former labmates and good colleague **Dr.**

Ritesh Prakash, Postdoctoral Fellow at the Institute of Quantum Biophysics, Sungkyunkwan University, South Korea, for always sharing his vast valuable knowledge in the multiphase domain, which greatly aided in my research work.

I would also like to express my fond gratitude to **Sir. T T Haokip**, Joint Registrar IIT Guwahati, and his family for their spiritual mentorship throughout my Ph.D. journey, which I will cherish forever. I am grateful to my friends, **Mr. Renben**, **Dr. Nzanthung**, **Er. Bonnie Deb Barma**, **IRS**, **Mr. Samuel**, **IRS**, **Dr. Azhoni**, **Dr. Ritho Chopi**, **Mr. Ari**, **Er. Venkatesh**, and **Mr. Rejulong** for their invaluable guidance and friendship. I cannot forget to thank my friends **Dr. Philip**, **Mr. Ato Kapfo**, **Mr. Charakho**, **Miss. Angukali, Mr. Varaprasad Gangadari**, **Miss. Sofia**, **Mr. Ado Khe**, **Mr. Alex**, **Miss. Khyo**, **Mr. Deep Anand**, **and Mr. Achan** for their great company during my stay in the campus.

I am indebted to **Miss. Rose**, whose unwavering support, patience, tolerance, and motivation have enabled me to achieved this dream. Thank you so much for everything you have done for me over the years. Words cannot express my gratitude to my in-laws, **Mr. Prem Bahadur**, DIS Rtd and **Mrs. Pitsala** for their unconditional love and support for me.

A special thanks to my beloved parents for always shouldering me through all the ups and downs of my life. I felt humbled and blessed to have such parents: my father, **Mr. Thrikyuba**, my mother, **Mrs. Tsijungla** and my siblings **Mrs. Achemla**, **Miss. Rithola**, **Miss Horipila**, **Mr. Lodomong**, and **Mr. Dumpilong**, this journey would be more difficult without their moral support. I would like to thank my brother-in-law, **Ps. Rangpi**, my cousin brothers **Ps. Kijung** and **Mr. Setrichem**, MD, for their unending moral support and prayers. Finally, I want to thank God for giving me good health and guiding me throughout my research journey. Your grace and blessings have been bestowed upon me.

Bongliba Sangtam

BRIEF BIODATA

Name:	**Bongliba T Sangtam**
Date of Birth:	**24/01/1992**
Phone Number:	**+91-7086550950**
Email:	**bonglibasangtam@gmail.com**
Ph.D	Indian Institute of Technology Guwahati, Guwahati – 781039, Assam, India
Years	2017 – 2022
Department/Specilization	Department of Chemical Engineering
M.Tech	Indian Institute of Technology Guwahati, Guwahati – 781039, Assam, India
Years:	2015 – 2017
Department/Specilization	Material Science and Technology, Department of Chemical Engineering
B.Tech	Coimbatore Institute of Technology, Coimbator – 641013, Tamil Naidu, India
Years:	2010 – 2014
Department/Specilization	Department of Chemical Engineering
Higher Secondary School	Edit Douglas Higher Secondary School Mokokchung – 798601, Nagaland
Years:	2008 – 2010
High School	Hill View Higher Secondary School Mokokchung – 798601, Nagaland
Years	2007 – 2008

AWARDS AND SCHOLARSHIP

- **MHRD Govt. of India scholarship for Ph.D. from July 2017 to July 2022**
- **MHRD Govt. of India scholarship for M.Tech from July 2015 to July 2017**

LIST OF JOURNAL PUBLICATIONS

- **Sangtam, B.T**., Prakash, R., Majumder, S.K., 2021. Drop sizes and its distribution in jet-driven liquid-liquid mixing column: Substantial application for the liquid-liquid extraction process. ***Chemical Engineering Research and Design***, 172, 186 – 203. doi.org/10.1016/j.cherd.2021.02.029
- **Sangtam, B.T**., Prakash, R., Majumder, S.K., 2021. Mixing characteristics of liquid-liquid dispersion in a jet-driven mixing column: Developed for separation of organic pollutants. ***Industrial & Engineering Chemistry Research***, 60, 18166 – 18182. doi.org/10.1021/acs.iecr.1c03733
- **Sangtam, B.T**., Majumder, S.K., 2020. Entrainment characteristic of liquid-liquid dispersion in a jet-driven mixing column: Substantial for process intensification in liquid-liquid extraction. ***Chemical Engineering and Processing:Process Intensification***, 153, 107927. doi.org/org/10.1016/j.cep.2020.107927

Other Publications

- Prakash, R., **Sangtam**, **B.T**., Hembrom K., Majumder, S.K., 2022. Bubble size analysis in a two-phase countercurrent flow in the narrow rectangular column. ***Physics of Fluids***, 34, 043305. https://doi.org/10.1080/10916466.2018.1482332
- **Sangtam, B.T**., Majumder, S.K., 2018. A new empirical correlation for prediction of gas hydrate dissociation equilibrium. ***Petroleum Science and Technology***, 36 (18), 1432 –1438. https://doi.org/10.1080/10916466.2018.1482332

Manuscript Under Review

- **Sangtam, B.T**., Majumder, S.K., 2022. Prediction of organic and inorganic gas hydrates equilibrium condition in the presence and absence of inhibitors. ***Petroleum Science and Technology*** **(Under Review)**. Manuscript ID: 223410339

Manuscript Under Preparation

- **Sangtam, B.T.**, Majumder, S.K., 2022. Investigation of extraction efficiency and overall mass transfer coefficient in liquid-liquid jet-driven extraction column.
- **Sangtam, B.T.,** Majumder, S.K., 2022. Quality of mixing in jet-driven liquid-liquid extraction column using information entropy.

Conference Publications

- **Sangtam, B.T**., Majumder, S.K., 2022. Extraction Efficiency and Mass Transfer of Carboxylic Acids Using Jetdriven Extraction Column. *North East Research Conclave*, *Indian Institute of Technology Guwahati*, Assam, India, May 20 – 22.
- **Sangtam, B.T**., Majumder, S.K., 2022. Dispersion Characteristic in Jet-driven Mixing Column and its Mechanism on the Turbulence and Circulation. *Research Conclave, Indian Institute of Technology Guwahati,* Assam, India, January 20 – 23.
- Prakash, R., **Sangtam, B.T**., Majumder, S.K., 2022. Effect of Surfactant Concentration and Gas Velocity on Holdup Characteristics in a Semi-batch 2-D column. *Proceedings of the 48th National Conference on Fluid Mechanics and Fluid Power (FMFP), Springer,* BITS Pilani, Pilani Campus, RJ, India, December 27 – 29.
- **Sangtam, B.T**., Majumder, S.K., 2021. Drop Aspect Ratio and Corresponding Correlation in Jet-driven Mixing Column. *CHEMCON-2021, CSIR Bhubaneswar,* India, December 27 – 30.

- **Sangtam, B.T**., Majumder, S.K., 2021. Drop Sizes Distribution and its Shape in Jet-driven Liquid-Liquid Mixing Column. *A Recent Trend in Fluid Dynamic Research (RTFDR-21),* NIT Rourkela, April 2 – 4.
- **Sangtam, B.T**., Majumder, S.K., 2021. Liquid-Liquid Dispersions in Intensified Jet-driven Mixing Column. *International Conference on Reaction Engineering (ICRE-21),* NIT Raipur, May 7 – 8.
- **Sangtam, B.T**., Majumder, S.K., 2019. Penetration of a Liquid Jet into Two Immiscible Liquid-liquid Dispersion in a Jet-driven Mixing Column. *Reflux 7.0, Annual Symposium Chem. Eng., Indian Institute of Technology Guwahati,* Assam, India, September 28 – 29.

ABSTRACT

Over the years, the research on the liquid-liquid plunging jet extraction column has drawn significant interest among the scientific fraternity because of its numerous applications, including fine chemical synthesis, recovery of fuel in nuclear plants, acid mixing, ink-jet, and liquid metal transfer (Asadollahzadeh et al., 2016; Gao et al., 2016; Hu et al., 2009; Tadrist et al., 1991). Various researchers have used different columns for the liquid-liquid extraction process such as Kühni column, rotating disc contactor, static mixer, and jet extraction column. Jet mixers have several advantages compared to mechanical mixers because they have low maintenance, low cost, low energy consumption, and shorter mixing time. The jet system has a higher liquid mixing and mass-transfer operation for mixing the liquid-liquid phase. For the past years, the jet device has been employed for wastewater treatment and acid extraction, but the studies were found to be limited. The jet device was used to extract copper ions, and it was discovered that the rate of copper extraction was 7 to 8 times higher than in the CSTR (Dehkordi, 2002a). Suresh et al. (2005) used liquid-liquid jet extraction system and separated uranium and thorium. They have stated that the ejector-type jet device can provide a high extraction efficiency. The various parameters such as liquid-liquid entrainment, drop size and its distribution, axial dispersion coefficient, extraction efficiency, and overall mass transfer play a significant role in designing and modeling of liquid-liquid extraction column. These parameters have an immense impact on selectivity and conversion in chemical engineering applications. Based on the literature, the jet-driven extraction column is gaining popularity for generating interfacial area, intense mass-transfer operations such as gas adsorption, liquid-liquid extraction, etc. However, there is a scarcity of studies on hydrodynamics and mass transfer for specific applications correlating the hydrodynamics in the jet-driven mixing column. The present work aims to enunciate hydrodynamics and its application in a jet-driven

liquid-liquid extraction column. As per the literature review and scope of the research, the following aims are framed under this main objective as:

- Entrainment characteristics of liquid-liquid dispersion
- Drop size distribution and drop aspect ratio
- Dispersion characteristics and its analysis
- Extraction efficiency and overall mass transfer in jet-driven extraction column

Chapter 2 presents the experimental investigation of the effects of the plunging of continuous liquid jets on a liquid-liquid dispersion of a two-phase system in a mixing column. The impact of various operating variables such as continuous liquid jets velocity, liquid jet lengths, mixture density, viscosity, and different dispersed phase volumes on immiscible liquid penetration heights were discussed. A mechanistic model was developed using the shell momentum balance and validated with the experimental data. A general correlation is developed based on the dimensional analysis to predict the penetration height at different operating variables.

Chapter 3 reports the study of drop size distribution, drop aspect ratio, and interfacial area in a liquid-liquid jet-driven column. Drop size distribution is found to follow the Log-logistic drop size distribution function. Empirical correlation is developed to predict Sauter mean drop diameter, drop aspect ratio, distribution function parameters, and interfacial area based on the operating variables and physical properties.

Chapter 4 focuses on studying the degree of liquid-liquid axial dispersion in a jet-driven mixing column. The effects of jet velocity and dispersed phase volume on mixing characteristics were studied. A general correlation was developed to predict the axial dispersion coefficient based on various operating variables. A mechanistic model was used to interpret dispersion due to turbulence and phase circulation inside the jet-driven mixing column. Based on the velocity

distribution model, the velocity characteristic factor and the dispersion factor of drop motion were also enunciated.

Chapter 5 studied the liquid-liquid extraction using solvents such as kerosene, diesel, 1-decanol, and paraffin in a jet-driven extraction column. The influence of jet velocity dispersed phase volume and physical properties on extraction efficiencies and mass transfer were studied. The overall mass transfer coefficient ($K_L a$) range was found to be 0.73 to 8.49 s^{-1} and 1.23 to 9.42 s^{-1}. A correlation is established based on the operating variables and physical parameters to predict the overall mass transfer coefficient.

Contents

LIST OF FIGURES

Chapter 1

Chapter 2

Chapter 3

Chapter 4

LIST OF TABLES

Chapter 2

Chapter 3

Chapter 4

CHAPTER 1

PREAMBLE AND RESEARCH WORK FORMULATION

1.1. Introduction

Multiphase flow is the simultaneous flow of two or more materials in different states or phases (such as gas, liquid, and solid) through a closed conduit. The multiphase flow reactors are the heart of any bulk chemicals industry, pharmaceuticals, fertilizer, polymer, and petrochemicals industry. There are several types of multiphase reactors or contractors, including the Kühni column (Oliveira et al., 2008), rotating disc contactor (Asadollahzadeh et al., 2017; Wang et al., 2002), static mixer (Voulgaropoulos et al., 2019), and jet extraction column (Dehkordi, 2002b; Gao et al., 2016). However, unlike other columns, the studies on hydrodynamic characteristics and mass transfer using the jet-driven liquid-liquid extraction column have received attention. The jet-driven column has the potential for process intensification in various chemical processes by entraining the liquid and forming interfaces to increase the interfacial area, especially in the liquid-liquid extraction process (Sangtam and Majumder, 2020). For the dispersion of air bubbles (Roy and Kumar, 2018), in the flotation process (Biń, 1993; Evans and Machniewski, 1999), downflow column (Majumder, 2016), nuclear reactor containment cooling system (Bertola et al., 2018), liquid metal transfer in the steel industry (Kirchner, 1974), spraying of water in agriculture and irrigation purpose (Eggers and Villermaux, 2008), and wastewater treatment (Kumar et al., 2018) this jet system can be used. Therefore, the study of plunging liquid-liquid jets becomes a significant application in various industries. In the last few years, different researchers have reported the study of mass transfer on liquid-liquid jet extraction columns (Asai et al., 1988; Dehkordi, 2002b; Fosberg and Heideger, 1967). However, there is limited literature based on a preliminary evaluation of hydrodynamic properties such as liquid-liquid entrainment, drop size and its distribution, drop aspect ratio,

interfacial area, and axial dispersion coefficient in jet liquid-liquid extraction columns. Liquid-liquid dispersion in jet-driven column received substantial attention in industrial applications as it has ability to produce finer drop size, higher dispersion efficiency, longer contact time for liquid droplets, greater interfacial area, and mass transfer than the conventional bubble column (Kumar et al., 2018; Roy and Kumar, 2018). An accurate interpretation of design parameters is essential for process modeling, operation, scale-up, and optimization of the system.

1.2. Design Parameters

The different design parameters, including liquid-liquid entrainment, drop size distribution, drop aspect ratio, mixing characteristic, and mass transfer are key elements for improving the efficiency of the liquid-liquid extraction column. All of these design parameters are interconnected. Various parameters and variables influencing the column performance are shown in Fig. 1.1. The process by which a liquid jet penetrates another immiscible liquid by plunging into its pool in a mixing column is known as liquid-liquid entrainment. Based on the height of the jet position and the flow Reynolds number, a dispersed droplet may entrain below the surface of the plunging jet (Majumder, 2016). Despite a thorough investigation of gas-liquid entrainment, knowledge of liquid-liquid entrainment remains limited. More research is required to fully comprehend the in-depth analysis of liquid-liquid entrainment at the impinging zone and the fluctuating interface at the plunging surface. The jet-driven mixing column has many advantages over traditional columns as it can disperse phases inside the column continuously without external force. Saito et al. (1988) and Park et al. (2001) conducted experimental studies of liquid jet plunging phenomena in different liquids such as water-freon-11, water-liquid nitrogen, water-fluorinert, and water-anatomic alloy system. They observed that the maximum penetration length is affected by the Froud number and the corresponding density and height of the liquid. In the present study, a jet-driven extraction column is designed, and the liquid-liquid entrainment characteristics are studied.

The entrainment of dispersion phase is essential for a critical design parameter for characterizing the hydrodynamics study in a jet-driven column. The current research investigates the phenomenon of immiscible liquid entrainment by the liquid jet in the mixing column in order to develop an efficient liquid-liquid extraction system based on process intensifications.

The knowledge of drop size and distribution is essential for analyzing system's performance for specific applications (Besagni et al., 2016; Khalil et al., 2010; Kumar and Hartland, 1996). These parameters have significantly impact the selectivity and conversion in a reactive system. The efficiency of the column is potently affected by the complex interaction of the phases. One of the essential parameters to consider when designing and optimizing an extraction column is the mean drop diameter and drop size distributions, which are crucial in the separation process (Amani et al., 2017). It impacts drop motion, residence time, dispersed phase holdup, interfacial area, and mass transfer (Hosseinzadeh et al., 2018). In various industries that involve liquid-liquid dispersion, drop size is essential in the solvent extraction process (Asadollahzadeh et al., 2015). Hosseinzadeh et al. (2018) studied the drop size distribution in the educator jet column and found that the nozzle diameter affects the drop size. In the water-kerosene system, it was noticed that as the liquid velocity increases, the drop size decreases (Samdavid et al., 2016). The mass transfer is controlled by the interfacial area of the dispersion in liquid-liquid extraction, which is the main parameter in the design and scaling-up of the separation column (Godfrey and Slater, 1994). The interfacial area influences the heat and mass transfer in the phase boundaries (Eastwood et al., 2004). As a result, assessing the interface rate of reaction and mass transfer between the phases requires a thorough understanding of the interfacial area between the liquid-liquid dispersion (Angle et al., 2006).

Multiphase reactor design requires a precise understanding of bubble or drop shape, which is necessary for measuring the gas-liquid interface transfer (Liu et al., 2021). Drop aspect ratio is

expressed as the ratio of a minor to a major drop axis. The shape of the drop size influences the drop's motion and heat or mass transfer (Clift et al., 1978). Understanding the aspect ratio is required for calculating the forces acting on the drop size and the mass transfer coefficient (Aoyama et al., 2016). Acharya et al. (1977) found that the drops form a spherical shape at low Re numbers, and at high Re numbers, the drop shape is distorted.

An understanding of the mixing characteristics is necessary for various chemical and biological methods to improve mass transfer efficiency and reduce side reactions caused by inappropriate concentration and temperature in the reaction vessel (Shadpoor et al., 2021). Increasing fluid mixing can eliminate dead zones inside the column vessel. In addition, knowing the proper mixing behavior can improve scale-up and modeling operations (Liu et al., 2008; Prończuk and Bizon, 2019). Backmixing is commonly observed in the extraction column, which reduces the efficiency of the column. It also occurs because of mixing density and friction caused by drop motions in the continuous phase. Backmixing can be estimated by the residence time distribution (RTD), the velocity distribution profile, and the dispersion number. It is determined by operating variables such as liquid flow rate and system geometry (Yerushalmi et al., 2013). The mixing phenomenon can be measured using the tracer technique and determined using an appropriate dispersion model. The residence time distribution (RTD) by conductivity measurement or tracer technique, is commonly used for studying the dispersion.

Mass transfer from a continuous phase droplet generally occurs in many industrial processes, particularly in liquid-liquid extraction and liquid phase reaction (Temos et al., 1996). In the industrial extraction process, one phase is used as the dispersed and the other as a continuous phase. This method can improve the interfacial area per unit volume for mass transfer by increasing the contact time between the phases. The degree of turbulence in the system and the interfacial area are important factors in improving the mass transfer efficiency of liquid-liquid contractors (Khooshechin et al., 2013). The high-intensity jet column outperforms other

conventional columns due to the high jet velocity impingement, resulting in intense mixing phases. The jet velocity increases the jet turbulence, which creates a strong shear force and thus enhances the interfacial area between the phases (Gao et al., 2016).

1.3. Industrial Significance of Jet Extraction Columns

Over the years, the jet mixer has been used as an alternative process to the impeller in the process industry. Jet turbulence can improve most industrial processes comprising chemical mixers, heat and mass transfer operations, drying, and combustion. Compared to a mechanical mixer, the jet mixing column can achieve higher turbulence, shear rates, low maintenance cost, and fewer moving parts. These jet mixers are also easier to operate than impellers (Wasewar, 2006). Often, the chemical reactions are carried out in stirred tanks, which results in nonuniform mixing and hence requires adequate additional strategies for efficient operation (Bhattacharya and Kresta, 2004).

On the other hand, the jet extraction column can generate strong turbulent energy dissipation more than the stirred tank (Siddiqui et al., 2009). The liquid from the nozzle jet is passed at a high jet velocity from the top of a column in the jet extraction column. The continuous liquid jet plunges inside the pool surface, causing intense mixing inside the column. When a continuous phase plunges over the surface of a dispersed phase, a droplet is formed inside the column.

1.4. Application of Jet-driven Extraction Column

The jet-driven extraction column has a wide range of practical applications. Some practical examples include:

- DSM Geleen in the Netherlands used jet aerators column for sewage wastewater treatment (Majumder, 2016).

- In the steel industry, liquid metal is transported from one container to another with the help of molten steel jets (Kirchner, 1974).
- A jet mixer is used to blend the inhibitors in the monomer storage tank (Hoffman, 1992).
- In a chemical reactor, the jet mixer is employed for an emergency cooling system (Schimetzek et al., 1994).
- For industrial applications, the jet mixer is used for hydrocarbon homogenization and LNG storage (Sarsten, 1972).
- Jet mixers are better suited for mixing chemically sensitive substances (Baldyga et al., 1995).
- Oil-jet lubrication is used to lubricate bearings in aviation engines and turbomachinery (Hu et al., 2014).
- During the welding process, the liquid metal jet is allowed to strike the weld pool (Soh et al., 2005).

1.5. Scope of the Research Work

Several studies have been conducted using various columns in the literature to elucidate the hydrodynamic characteristics and mass transfer in gas-liquid and gas-solid systems. But, research on liquid-liquid dispersion is still limited, particularly in the jet-driven extraction column. The jet extraction column can generate finer droplet size, dispersion efficiency, contact time, higher interfacial area, and mass transfer than the bubble column (Kumar et al., 2018). The liquid-liquid jet extraction process can be improved by increasing the interfacial area and the phase contact. The jet-driven liquid-liquid extraction column can be used to increase the interfacial area by generating smaller droplets, thereby improving the mass transfer efficiency. According to the literature review, no in-depth analysis based on the jet-driven liquid-liquid extraction column has been performed, indicating the influence of different operating variables,

physical properties, and geometrical variables on the hydrodynamic characteristics and mass transfer efficiency in the presence of different dispersed liquids.

1.6. Main Objective of the Present Research

The current study is developed based on a jet-driven extraction column for efficient liquid-liquid dispersion and its application in the liquid-liquid extraction process. The following sub-objectives are being studied, which are as follows:

- Liquid-liquid entrainment characteristics
- Drop size distribution and drop aspect ratio
- Mixing characteristics and its analysis
- Extraction efficiency and overall mass transfer coefficient

1.7. Thesis Structure

To understand the hydrodynamic behavior and its application for liquid-liquid extraction, the present work has been organized as follows:

Chapter 1: Introduction

This chapter presents an overview study, including a description of the liquid-liquid jet-driven extraction column, design parameters, industrial significance, applications, research gap, the scope of present work, key objectives, and the thesis structure.

Chapter 2: Liquid-liquid Entrainment Characteristics

This chapter reports the experimental investigation of the effects of the plunging of continuous liquid jets to produce fine droplets by entrainment of the other immiscible liquids. The phenomenon of liquid entrainment is explained in this work based on the experiment using kerosene-water, 1-decanol-water, paraffin-water, and soybean oil-water in the mixing column. The effects of a continuous liquid jet, length of jet, mixture density, mixture viscosity, and the

volume of different dispersed liquids on immiscible liquid penetration heights were discussed. A mechanistic model is developed and validated using the current experimental data. A general correlation is also developed for predicting jet penetration for intense dispersion based on various operating variables. A detailed study on liquid-liquid entrainment characteristics is described in Chapter 2.

Chapter 3: Drop Size Distribution and Drop Aspect Ratio

This chapter described the study of drop size distribution, drop aspect ratio, and interfacial area in a jet-driven mixing column. The influence of jet velocity, dispersed phase volume, liquid mixture density, and the viscosity of liquid mixture on the drop size distribution and drop aspect ratio were studied. Drop size distribution is fitted using Log-logistic, Beta, and Weibull distribution function, and the best fit was found to be Log-logistic model. For a small drop, the aspect ratio is closed to unity, and it decreases as the drop size increases. The increase in the Eötvös number leads to a decrease in the aspect ratio. The correlation for the drop aspect ratio is proposed in terms of the Reynolds and Eötvös numbers at the range of $0.061 < Re < 342.59$, $0.004 < Eo < 1.166$, and $(-4.756) < \log_{10}(Mo) < (-9.171)$, respectively. Interfacial area of drop enhances with an increase in the volume fraction of dispersed phase and jet velocity. Based on the current experimental data, a general correlation is developed for predicting the Sauter mean drop diameter, drop aspect ratio, distribution function parameter, and interfacial area based on operating variables and physical properties. A detailed study on drop size distributions, aspect ratio, and interfacial area is further discussed in chapter 3.

Chapter 4: Mixing Characteristics and its Analysis

This chapter investigated the degree of mixing characteristics of liquid-liquid in a jet-driven mixing column. The effects of jet velocity and dispersed phase volume on mixing characteristics were studied. The axial dispersion coefficient range was found to be 25.6 cm^2/s

to 106 cm^2/s. A general correlation was developed to predict the axial dispersion coefficient based on various operating variables. A mechanistic model was used to interpret dispersion due to turbulence and phase circulation inside the jet-driven mixing column. Based on the velocity distribution model, the velocity characteristic factor and the dispersion factor of drop motion were also enunciated. A detailed explanation of the mixing characteristics of liquid-liquid dispersion is examined in chapter 4.

Chapter 5: Extraction Efficiency and Overall Mass Transfer Coefficient

The chapter described the liquid-liquid extraction of acetic acid and propionic acid in water using kerosene, diesel, 1-decanol, and paraffin as the dispersed phases. The effects of jet velocity, dispersed phase volume, and various physical properties such as mixture density, viscosity, and surface tension on extraction efficiencies and overall mass transfer coefficients were investigated. The total mass transfer coefficient (K_La) was found to be 0.73 to 8.49 s^{-1} and 1.23 to 9.42 s^{-1}, respectively. A correlation is established based on the operating variables and physical parameters to predict the overall mass transfer coefficient. A comprehensive discussion on the extraction efficiency and overall mass transfer coefficient is presented in chapter 5.

Chapter 6: Overall Findings and Future Recommendation

This chapter covered the overall findings and recommendations based on the liquid-liquid jet-driven extraction column. It described the detailed studies of the hydrodynamic characteristics and mass transfer in a liquid-liquid jet-driven extraction column. Still, some research is needed to understand this area to construct, optimize, control, and scale up the column. As a result, this chapter discusses the possible future work in this research area.

CHAPTER 2

LIQUID-LIQUID ENTRAINMENT CHARACTERISTICS

Abstract

This chapter describes an experimental study of liquid-liquid entrainment characteristics in a jet-driven column. The comprehensive studies on the effects of jet velocity, dispersed phase volume, minimum jet velocity, and energy efficiency on penetration heights of the immiscible liquid are enunciated. A general correlation is also developed to predict jet penetration for intense dispersion based on various operating variables. A mechanistic model is derived and validated with the present experimental data.

2.1. Introduction

The liquid-liquid entrainment is the process in which a liquid jet penetrates another immiscible liquid by plunging into its pool in a mixing column. The entrainment of the liquid is very common in many practical interests, such as in the petroleum, pharmaceutical, and food processing industries for enhancing the interfacial area for mass transfer by producing the liquid droplets. Over the last few decades, extensive research work based on the gas-liquid entrainment system has been reported. Unlike the study of the gas-liquid system, the same has not been enacted in case of the liquid-liquid system. Though it is potential for the process intensification in various chemical processes to entrain the liquid and formation of interfaces to enhance the interfacial area, which is especially important for the liquid-liquid extraction process. The jet system can be used for the dispersion of air bubbles (Roy and Kumar, 2018), in the flotation process (Biń, 1993; Prakash et al., 2018), in downflow column reactors (Majumder, 2016), in nuclear reactor containment cooling system (Bertola et al., 2018), steel industry, spraying of water in agriculture and irrigation purpose, food industry, jet propulsion

(Eggers and Villermaux, 2008), and wastewater treatment (Kumar et al., 2018). In the welding process, the liquid metal is allowed to plunge into the weld pool. In the spray cooling system, the liquid jet is allowed to strike at the water surface (Soh et al., 2005). Therefore, the study of plunging liquid jet has become an interesting application in various industries. Saito et al. (1988) and Park et al. (2001) have performed a series of experimental studies of plunging phenomena of the liquid jet into various liquids such as water-freon-11, water-liquid nitrogen, water-fluorinert, and water-anatomic alloy system. Saito et al. (1988) have developed a semi-empirical equation for the prediction of jet penetration height for the coolant liquid, which tends to increase with increasing liquid jet velocity. Also, Park et al. (2001) reported that an isothermal plunging liquid jet into the pool of another liquid showed vigorous penetration of water into the fluorinert. They concluded that the maximum jet penetration depends on the Froude number and ratio of the density of the liquid jet and the pool liquid height. During the plunging process, the stability of a liquid jet depends on the jet velocity and jet geometry. The jet geometry depends on the nozzle diameter, jet length, physical properties of the liquid of jet (Burgess et al., 1972). The change in jet diameter depends on the fluid properties. Usually, the change of jet diameter encounters in industrial handling materials such as molten glass, plastics, cosmetics, paints, and food products (Zhu et al., 2000).

Kitamura et al. (1982) stated that in a vertical liquid jet, there is an effect of acceleration due to gravity on the break-up of liquid jet length. The break-up length is increased with increasing nozzle diameter. The plunging of a vertical jet system causes high momentum to enhance the liquid-liquid mixing in the column (Majumder, 2019). At the pool of free surface, when the liquid jet strikes, the concave shape of the mixing zone inside the column is formed. With the increase in the liquid jet velocity, the concave shape extends below the free liquid surface (Bin and Smith, 1982). Based on this phenomenon, the liquid entrainment of two and three-phase system in the downflow column were reported by various authors (Goshika and Majumder,

2018; Mandal et al., 2003; Sivaiah et al., 2012). Hammoumi et al. (2002) have studied the alcohol-water, lobelia TB15 oil-water, and glucose-water mixtures in the downflow liquid column. They have focused on the effects of the Weber number of entrainment and Öhnesorgue number for laminar and turbulent flows. Similarly, Lau et al. (2005) studied the degree of liquid entrainment in a high-pressure column with water and paratherm. It was reported that the rate of liquid entrainment increased with pressures and superficial gas velocities.

The present work aims to study the phenomena of entrainment of the immiscible liquid by the liquid jet in the mixing column for the development of an efficient liquid-liquid extraction system based on process intensifications.

2.2. Experimental Setup, Materials, and Methodology

2.2.1. Experimental Setup

The apparatus consists of a cylindrical column made up of transparent glass for clear visualization of flow. A strobe light is used to observe the liquid-liquid entrainment phenomena. The bypass control valve is used to minimize the turbulence effect hindering the liquid flow rate measurement. The liquid flow rate from the storage tank was monitored by using rotameter, and the edge of the pipe from the rotameter was connected to a nozzle. The dispersed liquid is fed into the top of the mixing column. The ratio of the nozzle length to nozzle diameter ($l_n/d_n = 5$) was kept constant. A nozzle supporter made of an aluminum frame is fixed to support the jet nozzle to prevent vibration during the operation of an experiment. The liquid level inside the column was maintained by a control valve at the bottom outlet of the mixing column. The detailed geometric dimensions of the experimental setup are shown in Table 2.1.

Table 2.1. Range of the experimental conditions.

Parameter	Range
Jet length(L_j)	0.213 – 0.227 m
Nozzle diameter (d_n)	0.005 m
Nozzle length (l_n)	0.025 m
Column diameter (d_c)	0.055 m
Column length (l_c)	0.37 m

2.2.2. Materials

For the present analysis, 1-decanol (with purity 98%) and paraffin liquid (with purity 98%) were purchased from Sigma-Aldrich and Himedia Laboratories Pvt. limited, respectively. Kerosene and soybean oil were locally purchased. The specific gravity bottle was used to measure the density of the water, and surface tension and viscosity of a dispersed liquid, Tensiometer (model: DY300; make: Kwoya, Japan) and Absolute viscometer (model: DV2TLVTJ0, make: BRK Instrument India LLP) were used.

2.2.3. The Estimation of Liquid-liquid Entrainment Rate

From the nozzle, the liquid jet was allowed at a certain flowrate to plunge vertically into the liquid-liquid solution to penetrate dispersed liquid inside the column. The jet length from the nozzle exit to the pool of the liquid surface was calculated based on the level of a mixture of the liquids in the column. The present study used water as a continuous liquid and kerosene, 1-decanol, and soybean oil as the dispersed liquid. The range of the dispersed liquid volume was considered within 2% – 8% according to the industrial application (Ritter and Kraume, 2000). All the experiments were performed at room temperature (301 K) and atmospheric pressure (1 atm). Liquid from the nozzle exit was allowed to plunge inside the column at velocities (u_j) within the range of 0.035 m/s to 0.283 m/s. In Fig 2.1, columns C_1, C_2, and C_3 were shown to indicate the penetration of dispersed liquid inside the column at different liquid jet velocities.

At a steady-state, the penetration height of dispersed liquid inside the column is captured using the high-speed digital camera (Phantom VEO 640 model, USA) with a resolution of 2560 ×1600 pixels. The images were recorded at the rate of 1400 frames per second. Further, the digital images are filtered, and the penetration height of the dispersed liquids was marked by using the image analysis software (Digimizer, version 4.2).

2.2.4. Physical Properties and Geometry of the System

In the present study, the water was taken as the continuous phase, while the kerosene, soybean, 1-decanol, and paraffin were taken as the dispersed phases. The mixture density is calculated by (Godfrey and Slater, 1994)

$$\rho_m = \rho_{dl}\varepsilon_{dl} + \rho_{cl}\left(1-\varepsilon_{dl}\right) \tag{2.1}$$

where ρ_m is the mixture density, ρ_{cl} and ρ_{dl} denote the liquid densities of the continuous and dispersed phases, respectively, and ε_{dl} is the dispersed phase volume fraction. The volume fraction of the dispersed phase is expressed (Tsaoulidis and Angeli, 2017) as

$$\varepsilon_{dl} = \frac{V_{dl}}{V_{cl}+V_{dl}} \tag{2.2}$$

where V_{cl} is the continuous phase volume, and V_{dl} is the dispersed phase volume. The mixture viscosity is calculated by (Godfrey and Slater, 1994)

$$\mu_{mix} = \frac{\mu_{cl}}{1-\varepsilon_{dl}}\left(1+\frac{6\mu_{dl}\varepsilon_{dl}}{\mu_{dl}+\left(1-\varepsilon_{dl}\right)}\right) \tag{2.3}$$

where μ_{cl} is the viscosity of a continuous phase, and μ_{dl} is the viscosity of a dispersed phase. Table 2.2 lists the physical properties of the liquids. For the surface tension (σ_m) of a liquid-liquid mixture, the following expression of Gliński et al. (2003) was used

$$\sigma_m = \frac{\sigma_{cl}\sigma_{dl}}{(1-\varepsilon_{dl})\sigma_{cl} + \varepsilon_{dl}\sigma_{dl}} \tag{2.4}$$

where σ_m, σ_{cl} and σ_{dl} are mixture surface tension, the surface tension of the continuous phase, and the dispersed phase surface tension, respectively. The ranges for the standard deviations, mean, and relative uncertainties are shown in Table 2.3. The detailed uncertainty analysis used in this study is presented in Appendix 1.

Table 2.2. Physical properties of the liquids at 298 K.

Liquid	Density (kg/m^3)	Surface tension (N/m)	Viscosity × 10^3 (kg/m s)
Water	998	0.071	1.00
Kerosene	810	0.034	1.56
1-decanol	828	0.028	11.07
Paraffin liquid	840	0.026	21.07
Soybean oil	916	0.033	47.25

Table 2.3. The uncertainty range of experimental data in the mixing column.

System	u_j (m/s)	$\bar{x}$	STDEV × 10^3	U	U_r (%)
Kerosene-water	0.035 – 0.283	0.027 – 0.070	3 – 2	1 – 1	5.369 – 1.650
1-decanol-water	0.035 – 0.283	0.024 – 0.067	4 – 2	2 – 2	8.567 – 1.803
Paraffin-water	0.035 – 0.283	0.022 – 0.065	3 – 2	2 – 1	7.898 – 1.776
Soybean oil-water	0.035 – 0.283	0.02 – 0.063	2 – 2	1 – 1	5.774 – 1.833

2.2.5. Models for Analyzing Penetration Height

The following correlation models are used to analyze the penetration height of liquid-liquid dispersion

2.2.5.1. Kramer et al. (2016) Model

Kramer et al. (2016) have analyzed the penetration heights of water jets using the artificial neural network tool. They have considered two variables: the momentum jet and the length of the jet. The general form of a model for the prediction of the penetration height of liquid jet was proposed as

$$H_p = aI^b L_j^{-c} \tag{2.5}$$

where *a*, *b,* and *c* are the coefficients that are obtained from the experiment. According to their experimental results, they have stated that the coefficients of *a, b, c* are 0.2, 0.39, and 0.26, respectively. Based on their experimental condition, they reported that the penetration heights of a liquid jet depend on the momentum of jet (*I*) at the plunging point, which is defined as

$$I = \rho_j Q_j u_j \tag{2.6}$$

where ρ_j is the density of jet, Q_j is the volumetric flow rate of a liquid jet, and u_j is the liquid jet velocity.

2.2.5.2. Friedman and Katz (1999) Model

To examine buoyancy force effects, Friedman and Katz (1999) presented the experimental study of two immiscible liquids (the water-diesel system where water was used as a jet). They have developed a general correlation for predicting the penetration height incorporating the effect of buoyancy force over the shear flow of the fluid, which is expressed by the Richardson number (*Ri*). The general form of correlation of the penetration height of a two immiscible liquid is

$$\frac{H_P}{d_n} = CRi^n \tag{2.7}$$

where C, n, and Ri are empirical constants and the Richardson number, respectively. From their experimental data, the values of C and n are found to be 0.75 and – 0.333, respectively. The values depend on the design of the system and fluid properties.

2.3. Results and Discussion

2.3.1. Mechanism of Liquid Entrainment

The liquid jet from the nozzle is penetrated into the denser liquid by the kinetic energy of the jet. As a result, the dispersed liquid as a droplet is entrapped into the pool of liquid into the column by penetrating the jet at a certain depth, which is called the penetration height.

For each experimental run at steady-state, the penetration height (H_p) of a jet into the pool of liquid is estimated by using a high-speed camera. The series of images indicates the liquid entrainment at a minimum liquid velocity of different dispersed phase volumes of 2% to 8% for various dispersed liquids such as kerosene, 1-decanol, paraffin, and soybean oil. Based on the different dispersed liquid volumes, the continuous liquid jet length was found to be varied with those variables. As the kerosene viscosity is lower, even at the higher concentration, the impingement of liquid jet is observed at the minimum liquid velocity u_j = 0.035 m/s. In case of 6% paraffin, 6 % soybean oil, 8% 1-decanol, 8% paraffin, and 8% soybean oil at low jet velocity u_j = 0.035 m/s, the liquid jet did not penetrate inside the pool of liquid in the column. The continuous liquid jet has an insufficient transfer of energy to break the surface of the dispersed phase above the surface of the pool of the liquid. Thus restrain to entrain the liquid jet into the dispersed phase inside the column. From the experimental condition, it is observed that the minimum liquid velocity increases with the increase in the viscosity of a dispersed liquid. At the same liquid jet velocity, it was observed that the density (number per unit volume)

of fine droplets was more in case of a kerosene-water system, which has a lower viscosity. At a higher liquid jet velocity (at u_j = 0.283 m/s), the jet plunged into the pool of the liquid in the column, the lower parts of the dispersed liquid oscillate, and it breaks into fine droplets due to high shear stress. Due to this, the liquid jet carries the dispersed liquid down the column. It was also observed that more fine droplets with uniform dispersion formed at high liquid jet velocity due to this entrainment.

2.3.2. Effect of Variables on Liquid-liquid Entrainment

2.3.2.1. Effect of Momentum Jet on Penetration Height

The effect of momentum jet on penetration height at a different dispersed volume of liquid is shown in Fig. 2.4. From the experimental conditions, it is observed that the penetration height and momentum jet increase with decreasing jet length at different dispersed volumes. With an increase in the liquid flow rate, the rate of the momentum jet increases, which leads to an increase in the penetration height (Parmar et al., 2015; Poling et al., 2001). The primary reason maybe because of the lower resistance by hydrodynamic interaction between the liquid jet and the kerosene, which increases the penetration heights with increasing momentum jet. For the other liquids, follow a similar trend of increase of the penetration height. As observed, even at a lower momentum of jet I = 0.005 kg m/s^2, there is a small penetration of kerosene inside the continuous phase of liquid. The same momentum of jet (I = 0.005 kg m/s^2) and the volume of the dispersed liquids of 1-decanol-water, paraffin-water, and soybean oil-water resulted in no penetration of dispersed liquids inside the column. The minimum penetration heights of 8% 1-decanol-water, 8% paraffin-water, and 8% soybean oil-water are observed at the momentum jet of I = 0.02 kg m/s^2. In the present system, as the density of kerosene is lower, the liquid jet easily penetrates the kerosene phase into the denser liquid even at a lower momentum of jet. From the experimental results, it is noticed that at a decreasing liquid jet length with increasing momentum, the penetration height of dispersed liquid increases. Also, the characteristic

relationship between the momentum jet and the penetration heights is found to be flattening at higher momentum jet (Kramer et al., 2016). The maximum penetration heights of kerosene, 1-decanol, paraffin, and soybean are found to be 0.70 m, 0.66 m, 0.65 m, and 0.63 m at the jet momentum of $I = 0.31$ kg m/s^2.

2.3.2.2. Effect of Viscosity on Liquid Entrainment

At lower dispersed volume liquids, the difference in the effects of a liquid jet on the entrainment is very small and results in the compactness of curves toward each other. Therefore, the effect of viscosity on penetration height at lower dispersed volume is insignificant in the present system.

It is observed that at the same volume of dispersed liquids, the penetration heights decrease with the decrease in Reynolds number. At minimum liquid velocity ($u_j = 0.035$ m/s), the liquid jet failed to penetrate through the volume of 6% paraffin and 6% soybean oil, resulting in insignificant liquid entrainment. With the increase in the volume of dispersed liquids, the apparent viscosity and density increase (Prakash et al., 2019). When the viscosity of the dispersed liquid increases, the hydrodynamic interactions between the dispersed phase and the continuous phase increases, and as a result, it lowers the penetration height. At the higher velocity of the liquid jet, the penetration heights increase with the increase in the volume of dispersed liquids. At low superficial liquid velocity $u_j = 0.035$ m/s and Re =163, the effect of kerosene viscosity on entrainment is negligible. At lower liquid velocity, the liquid jet favors the entrainment of the kerosene phase, while the jet failed to penetrate through the 1-decanol, paraffin, and soybean oil phase. Therefore, it is concluded that only at lower Reynolds number, the penetration height is affected by the change in viscosities.

2.3.3. Analysis of Entrainment Characteristics by Developing Models

2.3.3.1. Analysis of the Minimum Velocity of Liquid-liquid Entrainment

The continuous liquid from the nozzle jet strikes at the liquid-liquid pool surface inside the column. The minimum liquid flow rate at which the jet penetrates the pool surface and form the first liquid droplet is called minimum liquid jet velocity. To penetrate the liquid droplet downward, the jet momentum must be higher than the buoyancy of the dispersed liquid (Goshika and Majumder, 2018). Many authors have attempted the theoretical model for the prediction of minimum velocity for liquid entrainment (Majumder, 2016).

2.3.3.2. Analysis of Energy Efficiency for Liquid-liquid Entrainment

The knowledge of the energy efficiency of phase mixing is required for designing the plunging jet mixing column. It is required for the estimation of the transport parameter. In the jet penetrated mixing column, the continuous liquid jet impinged into the pool surface. As the dispersed liquid is penetrated by the plunging of liquid, dynamic pressure inside the column is developed depending on the rate of energy supplied by the liquid jet (Majumder, 2019). The rate of energy supplied to the mixing column can be expressed as

$$E_{sp} = \frac{1}{2}\dot{m}_j u_j^2 = \frac{1}{2}\rho_j Q_j u_j^2 \tag{2.11}$$

A fraction of the energy supplied is dissipated to overcome the friction of the liquid in the column. However, all the energy supplied is not utilized for mixing in the plunging region.

water, paraffin-water, and soybean oil-water decreases with the increase in the Reynolds number. It is because of the increase in the kinetic energy during the jet penetration inside the mixing zone. Also, with the increase in the volume of dispersed liquids, the mixing coefficient (K_m) decreases. Due to the higher viscous medium of the liquid-liquid mixture hinders the liquid jet from penetrating the mixing zone. So, it required more energy utilization for the

mixing of the liquid-liquid system. The energy utilization of liquid mixing in the mixing zone increase with the Reynolds number. It is because the rate of energy dissipation decreases with the increase in the Reynolds number. With an increase in the Reynolds number, the rate of turbulence energy of the liquid mixture increases. At higher turbulence, more energy utilization is required for the liquid jet to penetrate the dispersed liquid inside the mixing column. For the constant Reynolds number, the energy dissipation coefficient (K_m) decreases, resulting in an increase in energy utilization efficiency for mixing.

2.3.3.4. Prediction of Liquid Entrainment by Developing a Correlation Model

In the present study, an effort has been made to predict the penetration height by developing an empirical correlation based on operating variables. It is observed that the penetration height of dispersed liquid depends on the density of the mixture, the viscosity of a mixture, the surface tension of mixture, liquid jet velocity, acceleration due to gravity, and the length of the jet. Based on the experimental data, the general correlation is made by using dimensional analysis, which can be expressed as a function of variables as

$$H_p = f\left(\rho_m, \mu_m, \sigma_m, u_j, g, L_j\right) \tag{2.30}$$

Using Buckingham's pi theorem of dimensional analysis, it can be expressed as

$$\frac{H_p}{d_n} = \lambda\left(\frac{d_n u_j \rho_m}{\mu_m}\right)^a \left(\frac{\rho_m d_n u_j^2}{\sigma_m}\right)^b \left(\frac{u_j^2}{g d_n}\right)^c \left(L_j\right)^d \tag{2.31}$$

where λ, a, b, c, and d are the constant, which can be obtained by multiple regression analysis with experimental data. The empirical correlation yield as

$$\frac{H_p}{d_n} = 7.384\times10^{-3}\left(\frac{d_n u_j \rho_m}{\mu_m}\right)^{0.141} \left(\frac{\rho_m d_n u_j^2}{\sigma_m}\right)^{1.171} \left(\frac{u_j^2}{g d_n}\right)^{-1.058} \left(L_j\right)^{-5.087} \tag{2.32}$$

The Eq. (2.32) is valid within the ranges of:

$$50.259 \le \left(\frac{d_n u_j \rho_m}{\mu_m}\right) \le 1384.593;\ 8.889\times10^{-2} \le \left(\frac{\rho_m d_n u_j^2}{\sigma_m}\right) \le 5.943;\ 2.556\times10^{-2}\left(\frac{u_j^2}{g d_n}\right) \le 1.635$$

$$0.213 \le \left(L_j\right) \le 0.227$$

The mean absolute relative deviation (MARD) was calculated by (Miwa et al., 2018)

$$MARD = \frac{1}{N}\sum_{i=1}^{N} \frac{\left|\left(\frac{H_p}{d_n}(i)\right)_{Cal} - \left(\frac{H_p}{d_n}(i)\right)_{Exp}\right|}{\left(\frac{H_p}{d_n}(i)\right)_{Exp}} \times 100 \qquad (2.33)$$

The correlation coefficient and standard error were found to be 0.98 and 0.07. Equation (2.32) predicts the penetration height with the error range of ± 11% and the mean average relative deviation (MARD) of 5.298%. In order to check their range of validity, some of the available correlations from the literature were compared with the present experimental data.. A good prediction by the proposed correlation for penetration heights of various dispersed liquids is observed. The developed model by Kramer et al. (2016) is found to be well predicted with overall mean absolute relative deviation (MARD = 8.554%) in the present experimental data. Friedman and Katz (1999) correlation also showed a good agreement with the overall mean absolute relative deviation (MARD = 11.132%) from the present experimental condition.

The comparison of mean absolute relative deviation (MARD) between the experimental values and the present proposed model and correlation and the other correlations available in the open literature are shown in Table 2.4. The two correlations, Eq. (2.5) and Eq. (2.7) were compared with the present experimental data, and it was observed that the Kramer et al. (2016) correlation is found to be a better fit compared with the Friedman and Katz (1999) correlation with an overall mean absolute deviation of 8.554 % while the proposed correlations with Friedman and Katz (1999) was found to be 11.132 %.

2.4. Conclusions

The present work described the liquid-liquid entrainment characteristics in a cylindrical mixing column with kerosene-water, 1-decanol-water, paraffin-water, and soybean oil-water system. The variables such as the effects of initial liquid jet velocity, length of jet, the density of the liquid mixture, the viscosity of the mixture, and the volume of dispersed liquids were studied. It is observed that the initial liquid jet velocity depends on the viscosity of the dispersed liquid. Also, the effects of the momentum flow on penetration height depend on the jet length. The maximum penetration heights of kerosene, 1-decanol, paraffin, and soybean are found to be 0.70 m, 0.66 m, 0.65 m, and 0.63 m, respectively. Experimentally it is envisaged that the increase in the volume of the dispersed liquid increases the rate of energy dissipation in the mixing column. The penetration height is correlated with variables in terms of jet length to nozzle diameter, Reynolds number, Weber number, and the jet Froude number. The intensity of liquid-liquid dispersion is obtained as a function of flow resistance in the mixing column. From the present study, it is concluded that the penetration height of the liquid entrainment depends on the kinetic energy of the liquid jet and the system properties. The present proposed model and the correlation presented a good agreement with the experimental data within the error range of ±16.77 and ±11, respectively. This present study will be useful for further understanding and modeling of the multiphase flow, especially for the liquid-liquid extraction system.

CHAPTER 3

DROP SIZE DISTRIBUTION AND DROP ASPECT RATIO

Abstract

This chapter describes an experimental study of drop size distribution, drop aspect ratio, and interfacial area in a jet-driven liquid-liquid column. The effect of the jet velocity, the dispersed phase volume, and the physical properties on the drop size distribution and drop aspect ratio are studied. Compared to other dispersed liquids, the number density of drops in different dispersed media (under specific experimental conditions) demonstrates that paraffin liquid generates a significant number of drops. The correlation for the drop aspect ratio is proposed in terms of the Reynolds and Eötvös numbers, and its drop shape is shown in the Clift diagram, where both the spherical and ellipsoidal shape regimes are presented. Empirical correlation is developed to predict Sauter mean drop diameter, drop aspect ratio, distribution function parameters, and interfacial area based on the system's operating variables and physical properties.

3.1. Introduction

In the liquid-liquid dispersion process, when the continuous phase plunges over the surface of a dispersed phase, droplet formation occurs inside the column (Sangtam and Majumder, 2020). The dispersion system is a complex phenomenon because it involves simultaneous drop breakage and drops coalescence (Maaß et al., 2012). Under certain practical conditions, the dispersed drops are often tricky to identify and sometimes challenging to observe inside the column wall (Oliveira et al., 2008). Several factors, such as jet velocity, the volume of the dispersed phase, nozzle characteristics, physical characteristics, and column geometry are influenced by the dispersed drop size. Therefore, the knowledge of drop diameter and its distribution is essential to measure the system performance. The efficiency of the column is

potently affected by the complex interaction of the phases. The complex phase interaction has significantly influenced the drop size distribution, and it has an immense impact on selectivity and conversion in chemical engineering applications. Over a few decades, some researchers have reported the mass transfer studies in the jet-driven liquid-liquid extraction column (Asai et al., 1988; Dehkordi, 2001, 2002c; Fosberg and Heideger, 1967; Jamshidi et al., 2001). However, there is no information based on the preliminary review of hydrodynamic characteristics such as drop size and distribution, drop aspect ratio, and the interfacial area in jet-driven liquid-liquid extraction columns in the literature.

There are various techniques available to measure the drop size and its distribution by many researchers. The methods involve photographic, light scattering, laser scattering, doppler particle analyzer, and electrical methods (Alban et al., 2004; Chatzi et al., 1991; Greaves et al., 2008; Li et al., 2005; Maaß et al., 2011; Parmar et al., 2015; Prakash et al., 2020). The non-intrusive technique (i.e., photographic) is preferred compared to the intrusive (i.e., optical probe) technique because it does not disturb the fluid flow. One of the easiest methods to measure drop size is by drawing manually over the drop interface (Prakash et al., 2019).

The drop size and its distribution in the liquid-liquid jet extraction column play a vital role in the system design and performance (Khalil et al., 2010; Tsaoulidis and Angeli, 2017). Hosseinzadeh et al. (2018) studied the drop size in a liquid-liquid educator jet extractor column, where they have used water as a continuous phase and toluene as a dispersed phase. They have reported that the drop size strongly influences nozzle diameter. Samdavid et al. (2016) also studied using a downflow extraction column for the water-kerosene system. It was observed that the drop size distribution decreased with an increase in the liquid velocity. Tsaoulidis and Angeli (2017) used water and kerosene and performed the liquid-liquid drop size in the impinging jet column. They have observed that drop size is influenced by the liquid flowrate and the main channel column. Esmaeeli et al. (2020) studied liquid-liquid mass transfer

coefficient using an educator extractor column where water was used as the continuous phase and the gasoil as the dispersed phase. It was reported that the increase in the Sauter mean drop diameter and decreasing nozzle diameter increase the rate of overall mass transfer coefficient and the extraction efficiency. Based on the CFD modeling, the influence of drop rise velocity of water as continuous and toluene as dispersed phase was also studied by Hosseinzadeh et al. (2017). Siddiqui (2014) studied the effects of viscosity on the drop size of silicon oils, sunflower oil, and n-alkanes in the presence of water in a confined jet column. It is concluded that the drop size distribution of sunflower oil is wider than silicon oil, although both the oil has the same viscosity. The sunflower oil has lower equilibrium oil/water interfacial tension compared to 50 cP silicon oil. The oil having lower interfacial tension enables higher drop deformation and more uniform drop size.

The study of rising or falling of drops in a fluid medium is essential for both academic and practical interests (Wanchoo et al., 2003). Hydrodynamics of drops rising or falling liquid in the different systems were studied by various authors (Besagni and Inzoli, 2016; Dhindsa et al., 2020; Liu et al., 2016; Wanchoo et al., 2003; Ziqi et al., 2010). Wellek et al. (1966) stated that the spherical drop size shape depends on the velocity of the continuous phase and the interfacial forces. At lower Reynolds number, the drop shape remains as spherical, while at the higher Reynolds number, the drop shape distorted from a spherical drop. The aspect ratio (ψ) of drop indicates the shape of a drop. Wanchoo et al. (2003) studied the shape of the Newtonian liquid drop in a non-Newtonian liquid and observed that the shape of the drop was spherical at Eötvös number ($0.1 < Eo \leq 1$) and Reynolds number ($Re < 20$), while it is oblate at Eötvös number ($Eo = 1$) and Reynolds number ($Re \geq 20$). For aspect ratio ($1 \leq \psi \leq 10$) and Reynolds number ($Re < 1$), the drop shape is assumed to be prolate. Similarly, Sugihara et al. (2007) have proposed an aspect ratio range of ($0.5 < \psi < 1$) in case of low viscosity liquid for a single rising bubble in the water. Aoyama et al. (2016) have developed the correlations in terms of Eötvös

and Reynolds numbers for ellipsoidal bubbles in infinite stagnant clean liquids in the Morton number (Mo) range of $10^{-7} < Mo < 10^{-3}$. Myint et al. (2007) also studied the aspect ratio (in the range of $-11.6 \leq \log_{10}(Mo) \leq -0.9$) of a single drop-in silicon oil as a dispersed phase and water and glycerol as the continuous phase. They reported a higher scattered aspect ratio in the case of pure water. In contrast, the scattering of aspect ratio is low for the liquid-liquid mixture because of the extensive drop breakage due to the viscous effect. Most of the studies on aspect ratios are based on the gas-liquid system, and they have presented several correlations of aspect ratios (Aoyama et al., 2018, 2016; Besagni and Deen, 2020; Besagni and Inzoli, 2019, 2016; Legendre et al., 2012; Myint et al., 2007; Okawa et al., 2003; Raymond and Rosant, 2000; Sugihara et al., 2007; Wellek et al., 1966). So far, no studies on aspect ratio have been reported in the jet-driven liquid-liquid extraction column.

The knowledge of the interfacial area is essential to obtain the interphase reaction and mass transfer rate in the liquid-liquid jet extraction column (Angle and Hamza, 2006; Eastwood et al., 2004; Hemmati et al., 2015; Sechremeli et al., 2006). The interfacial area can be estimated based on physical and chemical methods (Majumder, 2019; Mandal, 2010; Van Woezik and Westerterp, 2000; Yang et al., 2011). Nosratinia et al. (2010) extracted succinic acid extraction using n-butanol as a dispersed phase jet extraction column. It is observed that with the increase in the height of the continuous phase, the interfacial area between the continuous phase and the length of the jet decreases, which in turn results in a sufficient time contact of solute between the continuous phase and dispersed phase. Dehkordi (2002c) used a high-intensity jet contractor for liquid-liquid jet extraction and studied the extraction efficiency and overall mass transfer coefficient of succinic acid, iodine, and acetic acid by using solvents as butanol, and kerosene, respectively. A high liquid jet velocity in a micro contractor volume subsequently causes an intense turbulence mixing of phases. The high shear forces acting on the liquid-liquid phase consequently increase the interfacial mass transfer area.

Based on the literature mentioned earlier, the present study focuses on an in-depth analysis of the influence of different dispersed liquid (i.e., kerosene, diesel, 1-decanol, and paraffin), jet velocities, the volume of dispersed liquid, viscosity, and surface tension on the drop size distribution, drop aspect ratio, and the interfacial area in the liquid-liquid jet-driven extraction column. New correlations are also proposed for drop diameter, drop aspect ratio, interfacial area, and distribution function parameters.

3.2. Materials and Methods

3.2.1. Materials

In this study, the chemical used was 1-decanol (purity 98%, Sigma-Aldrich, India), paraffin liquid (purity 98%, Himedia Laboratories Pvt. Limited, India). The kerosene and diesel were locally purchased at nearby gas station. The physical properties used in the current study are given in Table 3.1.

Table 3.1. Different physical properties of the liquid at 298 K.

Liquid	Density (kg/m^3)	Surface tension (N/m)	Viscosity $\times$ 10^3 (kg/m s)	Log_{10} (*Mo*)
Water	998	0.071	1	-10.957
Kerosene	810	0.025	1.56	-9.171
Diesel	819	0.028	3.16	-8.109
1-decanol	828	0.029	11.07	-5.986
Paraffin liquid	840	0.026	21.07	-4.756

3.2.2. Experimental Setup

All the experiments were performed at atmospheric pressure (1 atm) and room temperature (298 K). The transparent column was used for clear visualization of the drop images in the column. The measurement of a cylindrical column length and diameter was 0.37 m and 0.055 m, respectively. In the current study, water was used as a continuous phase, while kerosene, diesel, 1-decanol, and paraffin were used as the dispersed phase. The experiments were performed in the jet velocity (u_j) at a range of 0.68 to 1.71 m/s, and the dispersed phase concentration of 1% to 3%, as per the literature (Baldyga and Bourne, 1993; Ritter and Kraume, 2000). Pump (make: Crompton Greaves Ltd., 0.50 HP, 2780 RPM, 2.50 AMP) was used to supply the continuous liquid into the column. Throughout the experimental process, the initial liquid height was maintained at 0.19 m from the base of the column. The column was washed after each experiment to prevent the retention of any impurities that may hinder the experimental values. LED light source was used to identify the formation of liquid droplets in the column. The nozzle length and diameter were 0.025 m and 0.005 m, respectively. The ratio between nozzle length and diameter ($l_n/d_n = 5$) was kept constant throughout the experiments. The nozzle is fixed at the end of the pipe, and the liquid flow rate is controlled by using a calibrated liquid rotameter (make: Five stars, range of flowrate: 0 – 200 *l*/*h*; accuracy: ± 5 % of full range). A nozzle frame made up of aluminum was attached along the pipe to prevent vibration while performing the experiments. Table 2.1 in Chapter 2 provides a summary of the column dimensions.

3.2.3. Image Analysis Procedure

In the present study, the image analysis technique was used to measure the drop diameter. During the experiment, when the system reached the steady-state, the dispersed liquid drop was recorded by a high-speed camera (model: Phantom VEO 640, USA) with resolutions of 2560 ×1600 pixels at 1400 frames per second. The scale was attached to the column wall to calibrate

the image analysis software. The recorded videos were transferred to the computer via a data logger (supplied by the camera manufacturer). The black sheet was placed behind the column wall to avoid parallax deformation and improve the image quality. The light (make: Yongnuo, model: YN-600, 600 LED bulbs) source was focused on the column while recording the video. The captured videos were then converted into images using visible light communication (VLC media player) software. The image analysis technique involves several steps, such as image segmentation, brightness, and contrast adjustment. Out of several images for particular experimental conditions, the best quality image was selected and enhanced to mark the drop to determine the drop diameter using the image analysis software (Digimizer, Version 5.4.3). For each image, 200 – 300 drops were marked to estimate the Sauter mean drop diameter (d_{32}). For Sauter mean drop diameter, the following equation is used

$$d_{32} = \frac{\sum_{i=1}^{n} n_i d_d^3}{\sum_{i=1}^{n} n_i d_d^2} \tag{3.1}$$

where n_i is the number of drops size of diameter d_d. For the elliptical shape drop, the equivalent drop diameter (d_{eq}) was determined by estimating the major (l_{maj}) and minor (l_{min}) axis of the drop.(Majumder, 2016)

$$d_{eq} = \sqrt[3]{l_{maj}^2 l_{min}} \tag{3.2}$$

The various physical properties such as liquid viscosity, equivalent drop diameter, surface tension, the density difference ($\rho_{cl} - \rho_{dl}$), and the acceleration due to gravity are the significant aspects that influence the drop diameter and its shape. As the continuous jet velocity increases, the droplet of dispersed liquid undergoes deformation and fragmentation; thus, a more substantial drop disintegrates into small droplets (Berna et al., 2015). It is clearly shown that at a low jet velocity, an aggregate structure resembling a honeycomb shape is formed, and it is made up of water encapsulated by a thin film of dispersed liquid (Samdavid et al., 2016). As

the continuous jet velocity increases, the drop distorts and splits into a small drop. The water as a higher density it escaped from the outer film of a dispersed liquid and left the dispersed film to form liquid droplets in the column. As a result, the drop collisions frequency increases, resulting in the breakage of dispersed liquids into uniform small drop size. The detailed physical properties and geometry of the system are presented in chapter 2 (section 2.2.4).

3.3. Results and Discussion

3.3.1. Effect of Different Variables on Drop Size

3.3.1.1. Effect of Jet Velocity on Sauter Mean Drop Diameter

It is observed that the Sauter mean drop diameter decreases for all the dispersed liquids as the jet velocity increases. It is attributed to the breakup of a large drop into a small diameter as the liquid jet plunging velocity increases. For each system, it was also noticed that the Sauter mean drop diameter was lower at dispersed phase volume of 3% in comparison to that of 2% and 1%. At a high dispersed phase concentration, the liquid-liquid mixture viscosity is more compared to the low concentration of the dispersed liquid.

A high viscosity liquid lengthens the coalescence rate of a drop; therefore, the drop size is small at a high dispersed liquid concentration. For dispersed volume (V_{dl} = 1.0%) at low velocity (u_j = 0.68 m/s), the Sauter mean drop size (d_{32}) is found to 2.52 mm and at high jet velocity (u_j = 1.71 m/s) the d_{32} reduced to 1.43 mm, the reduction is about 43.20%, while (at V_{dl} = 2.0%) the reduction of d_{32} for 0.68< u_j < 1.71 m/s is 41.77%, and in the case of (V_{dl} = 3.0%) the reduction within the same jet velocity is found to 40.26% (as shown in Fig. 3.4a). It is also observed that the average reduction in the Sauter mean drop diameter of kerosene (at 2.0% and 3.0%) at jet velocity range of 0.68< u_j < 1.71 m/s is 48.61%. For the diesel-water system, at low jet velocity (u_j = 0.68 m/s) the d_{32} was 2.41 mm (at V_{dl} = 1.0%) and with increase in liquid jet (u_j = 1.71 m/s) the d_{32} decreases to 1.28 mm, the reduction of size within the jet velocity of 0.68< u_j <

1.71 m/s is 46.86% as shown in Fig. 3.4b. For the 2.0% and 3.0% volume of diesel at jet velocity 0.68< u_j < 1.71 m/s, the average reduction of drop diameter is 45.23%. A similar trend was observed in 1-decanol and paraffin systems, as shown in Fig. 3.4c, and Fig. 3.4d. In case of 1-decanol and paraffin, the average reduction for 2% and 3% volume at the same jet velocity range is found to 36.42% and 25.81%, respectively. The Sauter mean drop diameter decreases with an increase in the jet velocity and dispersed liquid volume. An increase in the momentum jet velocity increases the shear, and as a result, the more intense mixing of liquid-liquid takes place, which breaks more drops into smaller sizes (De Hert and Rodgers, 2017; Tsaoulidis and Angeli, 2017).

3.3.1.2. Effect of the Volume of Dispersed Liquid on Sauter Mean Drop Diameter

At lower jet velocity (u_j = 0.68 m/s) the order of d_{32} in different dispersed liquid (at V_{dl} = 1% to 3%) are: d_{32} (kerosene) > d_{32} (diesel) > d_{32} (1- decanol) > d_{32} (paraffin). An increase in the dispersed phase viscosity and density increases the hydrodynamic interaction between the continuous liquid velocity and the dispersed liquid, thus decreasing the drop breakage. In the present study, it is noticed that at lower jet velocity (u_j = 0.68 and 1.02 m/s), the kinetic energy of the liquid jet failed to break the dispersed liquids drops, and thus, the obtained drops are more irregular shapes. The force that changes the drop diameter is due to the dynamic jet and viscous forces on the liquid mixture surface (Karam and Billinger, 1960). It is observed that the Sauter mean drop diameter decreases with an increase in jet velocity. Similarly, at higher jet velocity (u_j = 1.02 and 1.71 m/s), the shear force increases and breaks the dispersed phase into uniform smaller drops by force associated with the continuous phase turbulence (Oliveira et al., 2008).

It is noticed that at higher liquid velocity jet (u_j =1.71 m/s), the drop breakage is independent of the viscosity of the dispersed liquid system, and due to this, a number of finer drop sizes are formed inside the column. It is seen that at the lower jet velocity, there is an influence of dispersed liquid on Sauter mean drop diameter. In comparison, at the higher jet velocity, it is independent of the liquid-liquid system.

3.3.2. Development of an Empirical Correlation and Comparison of Experimental Data with Literature Correlation

In current experimental conditions, an empirical correlation is developed to predict the Sauter mean drop size in the jet-driven liquid-liquid mixing column. It is seen that the various parameters such as the liquid jet velocity, nozzle diameter, mixture liquid density, mixture liquid viscosity, mixture liquid surface tension, and acceleration due to gravity influenced the drop size. Therefore, all these parameters are considered for the development of an empirical correlation. For developing an empirical correlation, the experimental values are evaluated based on the Sauter mean drop diameter (d_{32}) as a function of a different parameter, which is expressed as

$$d_{32} = f\left(u_j, d_n, \rho_m, \mu_m, \sigma_m, g\right) \tag{3.3}$$

By applying Buckingham's pi theorem, it follows

$$\frac{d_{32}}{d_n} = \omega\left(\frac{d_n u_j \rho_m}{\mu_m}\right)^a \left(\frac{u^2{}_j d_n \rho_m}{\sigma_m}\right)^b \tag{3.4}$$

where ω, a, and b are constant parameters that are obtained by the regression analysis method. For a jet-driven column, the proposed correlation for Sauter mean drop size is expressed as

$$\frac{d_{32}}{d_n} = 2.368\times10^{-8}\left(\frac{d_n u_j \rho_m}{\mu_m}\right)^{2.817}\left(\frac{u_j^2 d_n \rho_m}{\sigma_m}\right)^{-1.709} \tag{3.5}$$

Equation (3.5) is valid within the ranges of $2505 \le d_n u_j \rho_m / \mu_m \le 6963$; $26 \le u_j d_n \rho_m / \sigma_m \le 175$. Equation (3.5) is coherent with the current experimental result with the correlation coefficient and standard error of 0.94 and 0.08, respectively. The proposed correlation (Eq. 3.5) has predicted the d_{32} with an absolute average relative deviation (AARD) of 6.75%.

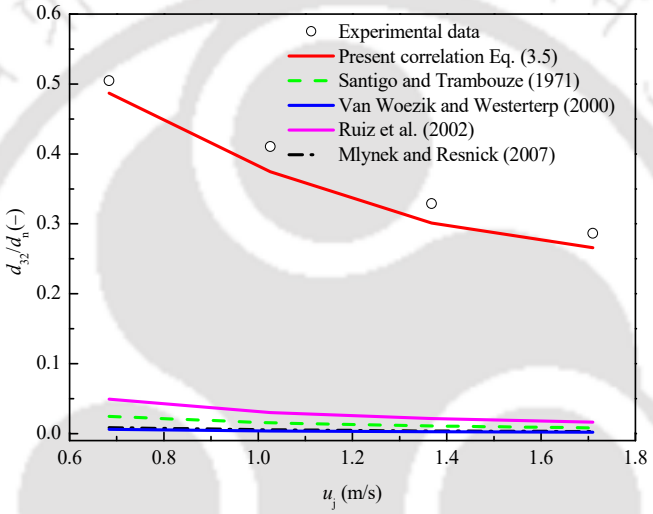

Figure 3.1. Correlation comparison based on the effects of liquid jet velocities on Sauter mean drop diameter.

The developed relationship predicts the d_{32} within the error range of ± 17.21%. The experimental values for d_{32} are also compared with the different correlations (Mlynek and Resnick, 1972; Ruiz et al., 2002; Santiago and Trambouze, 1971; Van Woezik and Westerterp, 2000), as shown in Fig. 3.6. It is observed that all these correlations are found to be under-predicted with the present experimental values. One of the main reasons may be that these correlations are based on different geometric dimensions, and therefore it is difficult to predict a specific system (Asadollahzadeh et al., 2016; Hosseinzadeh et al., 2018).

3.4. Conclusions

The present work reports the hydrodynamic characteristics such as drop size distribution, aspect ratio, and interfacial area in a jet-driven liquid-liquid extraction column. Four different liquids (kerosene, diesel, 1-decanol, and paraffin) are used as the dispersed medium, while the water is used as the continuous phase. The influences of jet velocity, the volume fraction of the dispersed phase, and the system's physical properties are studied. Based on the experimental analysis, the following conclusions are drawn:

- Drop size and its distribution is greatly influenced by the operating variables and physical properties of the system. With an increase in the jet velocity and dispersed phase volume, the drop size reduces significantly. The drop size distribution is wider at lower jet velocity and dispersed phase volume. In the current system, the drop size distribution fits the Log-logistic distribution function model with the least error. The observed order of drop size (d_{32}) in the present experimental conditions is: d_{32} (kerosene) > d_{32} (diesel) > d_{32} (1-decanol) > d_{32} (paraffin).

- The influence of drop diameter on the interfacial area is more pronounced in comparison to that of the volume fraction of dispersed liquid. The order of interfacial area for different dispersed liquids are a_i (paraffin) > a_i (1-decanol) > a_i (diesel) > a_i (kerosene).

- Drop aspect ratio is close to 1 at lower Eötvös number and decreases significantly as the Eötvös number increases. The relative frequency of drops having aspect ratio $0.9 \le \psi \le 1.0$ increases with an increase in the jet velocity and dispersed phase volume. It indicates that the sphericity increases with the jet velocity and dispersed phase volume. Correlations are developed for aspect ratio in terms of Eötvös and Reynold's number.

CHAPTER 4

MIXING CHARACTERISTICS AND ITS ANALYSIS

Abstract

This chapter focuses on studying the degree of liquid-liquid axial dispersion in a jet-driven mixing column. The effects of jet velocity and dispersed phase volume on mixing characteristics were studied. A general correlation is developed to predict the axial dispersion coefficient based on various operating variables. A mechanistic model is proposed to interpret dispersion due to turbulence and phase circulation inside the jet-driven mixing column. Based on the velocity distribution model, the velocity characteristic factor and the dispersion factor of drop motion were also enunciated.

4.1. Introduction

Backmixing commonly occurs in most extraction columns, affecting the column extraction efficiency. Backmixing in the continuous phase may result from the differences in mixture density or the friction obtained in moving bubbles/drops that carry some continuous phase along with them. Backmixing also affects reaction rates and selectivity for various degrees in multiphase reactors (Shah et al., 1978). In a confined jet, the liquid mixing depends on recirculation, which is strongly influenced by turbulent dispersion (Moeller and Dealy, 1970). The energy efficiency of jet mixing is governed by the relative energy distribution between the convective and turbulent dispersion (Patwardhan and Gaikwad, 2003). When the liquid jet plunges into the pool of liquid in the column, the turbulent mixing occurs by the entrainment of gas by the liquid jet (Rajaratnam, 1976). The backmixing can be assessed using the residence time distribution, the velocity distribution profile, and the dispersion number. It depends on the operating variables, such as liquid flowrate and system geometries (Yerushalmi et al., 2013).

The mixing phenomena can be measured using the tracer technique, and it can be determined by using an appropriate dispersion model. Residence time distribution depends on the flow characteristics and system geometry and influences the system performance (Fogler, 2016; Levenspiel, 1999; Tsaoulidis and Angeli, 2017). It also interprets the degree of backmixing, kinetics model and improves the reactor design with a specific flow pattern (Fogler, 2016; Levenspiel, 1999). In the literature, most of the studies on liquid-liquid jet mixing systems focused on mass transfer characteristics; however, the hydrodynamic mixing characteristics were neglected (Tsaoulidis and Angeli, 2017). Dehkordi (2001) and Nosratinia et al. (2010) used a jet system and studied the mass transfer operation to extract the solute, but they did not investigate the hydrodynamic characteristics. Saien and Moradi (2012) used butanol for mass transfer studies of succinic acid in the aqueous phase by varying the jet systems such as nozzle diameters, nozzle lengths, and jet velocities. They have obtained a high mass transfer rate at a minimum energy dissipation compared to other types of extraction columns.

In the past few decades, extraction columns were designed based on the assumption that each phase follows the ideal plug flow model. However, various studies have been conducted to estimate the deviation of nonideality from ideal plug flow conditions caused by liquid circulation, eddies, turbulence, and velocity profile (Kumar and Hartland, 1999; Morales et al., 2007). These parameters were combined into a single parameter based on Fick's law, and it is expressed as the axial dispersion model (Danckwerts, 1953). Taylor (1954) first studied the axial dispersion model for turbulent mass transfer through a pipe. The liquid flow is assumed to be perfectly mixed along the lateral axis perpendicular to the liquid flow direction. Huang et al. (2018) examined the mixing properties of an air-water system in a jet bubbling reactor using the tank series model and the axial dispersion model. Ikeda and Suzuki (1991) also studied the axial mixing coefficient in the nozzle plate column using water as the continuous phase and kerosene as the dispersed phase. They observed that the flow pattern inside the column for the

dispersed phase was different from the continuous phase. The influence of jet, conductivity probe location, and jet Reynolds number on mixing time was studied by Amiri et al. (2011). It was reported that the mixing time decreases with an increase in the jet velocity at a constant nozzle diameter. Velan and Ramanujam (1994) investigated the mixing characteristics of Newtonian and non-Newtonian fluids in a downflow jet loop bioreactor. It was reported that as the liquid flow rate increases, the axial dispersion coefficient increases. Ayass et al. (2016) performed an experiment to measure the overall mixing in jet-stirred reactors passively mixed by feed nozzles. An intense liquid circulation was formed inside the column when the nozzle jet angle was kept at 45°, which enhanced the mixing (Rahimi and Parvareh, 2005). The nozzle jet position influences the rate of mixing performance (Parvareh et al., 2009). As per literature, the jet-driven mixing column is gaining importance as a mixing column which is very useful for interfacial area generation for intense mass transfer operations like gas- adsorption, liquid-liquid extraction, etc. However, there is a lack of studies on hydrodynamics and analysis of mass transfer for specific applications correlating the hydrodynamics in the jet-driven mixing column.

The present work is intended to enunciate the influence of the system operating variables and physical properties on the axial dispersion in the jet-driven mixing column. In addition, the axial dispersion coefficient of the system is analyzed using the velocity distribution model. A mechanistic model was also developed to interpret the dispersion by circulation, dispersion resulting from turbulence, and liquid exchange parameters.

4.2. Theoretical Analysis

4.2.1. Kinetics of Mixing by Dispersion Model

The proper mixing of liquid-liquid dispersion is essential to increase the high yield of reaction and the column performance. The continuous phase plunges into the surface of the stationary

liquid from the nozzle, and intense mixing occurs inside the column. The axial dispersion model, which describes the distribution of tracer overtime to interpret the intensity of mixing in the column, can be expressed as (Fogler, 2016)

$$\frac{\partial C}{\partial t} = E_d \frac{\partial^2 C}{\partial l^2} - \frac{u_j}{1-\varepsilon_{dl}} \frac{\partial C}{\partial l} \tag{4.1}$$

where C is the tracer concentration, t is time, and l is the distance between the tracer inlet and the detector point. The following expression is the dimensionless form of Eq. (4.1)

$$\frac{\partial C_\theta(z,\theta)}{\partial \theta} = \frac{1}{Pe} \frac{\partial^2 C_\theta(z,\theta)}{\partial z^2} - \frac{\partial C_\theta(z,\theta)}{\partial z} \tag{4.2}$$

where $C_\theta = \frac{C}{C_0}$; $\theta = t / t_m$, $t_m = l/u_j$ and $z = l/L$

$$Pe = \frac{u_j z}{(1-\varepsilon_{dl}) E_d} \tag{4.3}$$

$Pe \to 0$ implies the system is perfectly mixed, whereas $Pe \to \infty$ refers to there is no dispersion, a plug flow behavior. In a column with a diameter less than 5 cm, the effect of radial distribution along the column is considered negligible compared to axial dispersion (Rubio et al., 2004). For a closed-closed system, the axial dispersion coefficient (ADC) for the liquid-liquid dispersion is expressed as

$$E_d = \frac{u_j z}{(1-\varepsilon_{dl}) Pe} \tag{4.4}$$

The Peclet number associated with variance (second moment of Eq. (4.2) and the mean residence time (first moment of Eq. (4.2)) is expressed as

$$\sigma_\theta^2 = \frac{\sigma^2}{t_m^2} = \frac{2}{Pe}\left[1 - \frac{1}{Pe}\left[1 - e^{-Pe}\right]\right] \tag{4.5}$$

where σ^2, t_m, and σ_θ^2 refer to the variance of the RTD curve, mean residence time, and the dimensionless variance, respectively. The exit age distribution (E) is the distribution of liquid time exiting the column. The exit age distribution can be obtained from the tracer concentration-time data. The exit age distribution (E) function is defined as (Fogler, 2016)

$$E(t) = \frac{C(t)}{\int_0^\infty C(t)\,dt} \tag{4.6}$$

where $C(t)$ (kg/m^3) is the tracer concentration at time t. The first and second moments represent the mean residence time (t_m) and the variance (σ^2), respectively. The mean residence time (t_m) and the variance (σ^2) are expressed by Eq. (4.7) and (4.8), respectively.

$$t_m = \frac{\sum tC\Delta t}{\sum C\Delta t} \tag{4.7}$$

$$\sigma^2 = \frac{\sum (t - t_m)^2 C\Delta t}{\sum C\Delta t} \tag{4.8}$$

4.2.2. Analysis of Liquid-liquid Dispersion by the Velocity Distribution Model

The velocity distribution model, dispersion due to drop motion, and the velocity characteristic factor influence the performance of a jet-driven mixing column. The mixing of liquid occurs due to the jet velocity and the drop motion in the column. A homogenous mixture is formed when a solute is transferred through a stream at a non-uniform velocity (Taylor, 1953). The axial dispersion coefficient (ADC) was used for the dispersed phase inside the jet-driven

mixing column, which can be determined using the velocity distribution model suggested as (Aris, 1956; Taylor, 1953)

$$E_d = \frac{d_c^2 u_j^2}{kD_s} + D_s \tag{4.9}$$

where D_s, k, and u_j are the molecular diffusivities, velocity characteristic factor, and the maximum velocity at the column axis. In the present study, Eq. (4.9) is used for analyzing the ADC of drop motion inside the jet-driven mixing column. D_s in Eq. (4.9) is replaced by the D_d of a drop motion, and it is expressed as

$$E_d = \frac{d_c^2 u_j^2}{kD_d} + D_d \tag{4.10}$$

From the slope and intercept, the velocity characteristic factor (k) can be calculated by

$$k = \left[\text{slope} \times \text{intercept}\right]^{-1} = \left[\frac{1}{kD_d} \times D_d\right]^{-1} \tag{4.11}$$

4.3. Experimental

For the current study, the continuous phase used was water, and the dispersed phase was kerosene, diesel, 1-decanol, and paraffin. The jet velocity and the dispersed phase volume range were 0.68 m/s to 1.64 m/s and 1.0% to 3.0%, respectively. Initially, in the column, the height of the liquid was kept at 0.28 m.

The liquid flowrate was controlled by a liquid rotameter (make: Five stars, range 0 – 200 l/h; accuracy: ± 5% of the full range). The column was cleaned after each experiment to avoid traces of the chemicals from the previous experiments. The water coils are also jacketed around the column to maintain the liquid temperature constant in the column. An aluminum frame is attached to a nozzle jet to avoid any disturbance of the liquid flow. The online conductivity

probe was used to measure the tracer concentration at different axial locations. The conductivity probe was installed in column D_4 for the present study. Columns D_1 to D_3, as shown in Fig. 4.1, represent the formation of a droplet and its dispersion with an increase in jet velocity. The tracer is injected from the top of the column, and the tracer concentration is measured at different axial locations using conductivity probes.

Table 4.1. Uncertainty ranges for experimental values.

Variables	Mean, $\overline{x} \times 10^2$ (m^2/s)	STDEV $\times$ 10^2 (–)	$U \times 10^2$ (–)	U_r (%)
E_d (kerosene-water)	0.257 – 3.459	0.017 – 5.175	0.010 – 2.982	3.936 – 8.638
E_d (diesel-water)	0.251 – 0.942	0.044 – 0.059	0.025 – 0.034	3.662 – 10.066
E_d (1-decanol-water)	0.280 – 1.363	0.027 – 0.037	0.016 – 0.215	5.669 – 15.802
E_d (paraffin-water)	0.323 – 1.330	0.025 – 0.245	0.014 – 0.142	4.494 – 10.659
u_j	*67.660 –165	7.094 – 10.532	4.096 – 6.083	3.686 – 6.053

*unit is in m/s.

Table 4.2. The value of slope for the calibration curves at different dispersed phases.

Dispersed phase	Concentration (vol. %)	y ($(kg/m^3).cm/mS$)
Kerosene-water	1	0.907
	2	1.027
	3	1.164
Diesel-water	1	0.889
	2	0.934
	3	0.943
	1	0.941

1-decanol-water	2	1.047
	3	1.027
	1	0.873
Paraffin-water	2	0.941
	3	0.951

The detailed physical properties and geometry of the system were presented in chapter 2 (section 2.2.4). Also, the physical properties used in the current study were given in chapter 3 (in Table 3.1). The schematic diagram of a nozzle and the conductivity probe is shown in Fig. 4.2a to 4.2b, respectively. The conductivity meters (make: Microset, model: MS CD 18) are attached to the data logger and a digital indicator, which is shown in Fig. 4.2c. The data logger was further attached to a computer through a RS 485 cable port. The conductivity meter ranges from 0 –19.99 mS/cm was used. Probes 1, 2, and 3 are located from the tracer inlet at a distance of 0.205 m, 0.135 m, and 0.065 m, respectively. The aspect ratio (l/d_c) of the location of the conductivity probe at the top section is 3.73, the middle is 2.45, and the bottom is 1.18. Initially, the conductivity meter was calibrated by preparing different NaCl solutions, and the conductivity of the water used was 0.12 mS/cm. A typical calibration plot of concentration is shown in Fig. 4.3. The different ranges of mean, standard deviation, and the relative uncertainty of the experiment are shown in Table 4.2. The following expression is used to calculate the solution concentration

$$C = y\left(K_c - K_w\right) \tag{4.12}$$

where C is the tracer concentration (kg/m^3), y in Eq. (4.12) is the slope, K_c is the solution conductivity (mS/cm), and K_w is the water conductivity. The values of the slope for different dispersed phases are shown in Table 4.3.

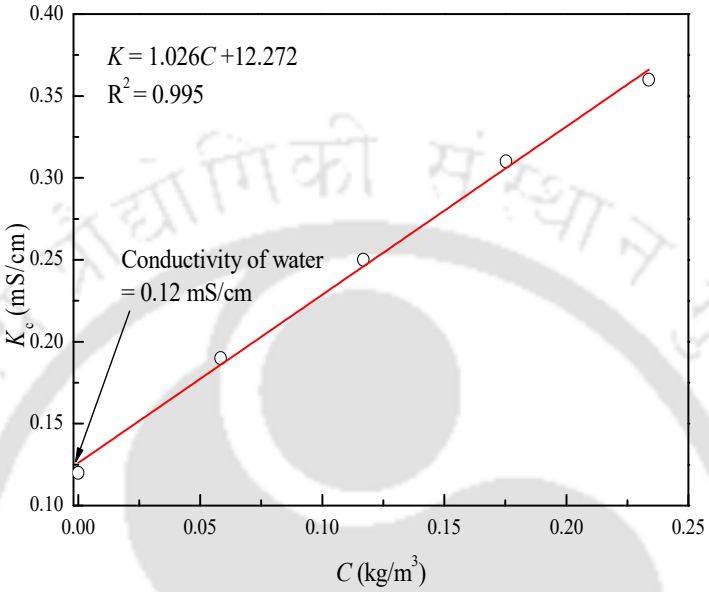

Figure 4.1. Typical calibration plot of the conductivity meter.

4.4. Results and Discussion

The effects of different operating variables on the mixing intensity are discussed in the following sections.

4.4.1. Effect of Sauter Mean Drop Diameter on Axial Dispersion Coefficient

The mixing phenomenon is influenced by the Sauter mean drop diameter (d_{32}) in a jet-driven mixing column. The comprehensive elucidations of Sauter mean drop diameter used in this work are shown in Chapter 2. The effect of Sauter mean drop diameter (d_{32}) on axial dispersion coefficient (E_d) at different dispersed phase volumes (kerosene-water) is shown in Fig. 4.4. It is observed that E_d decreases as d_{32} increases for all the dispersed phase volumes. The reduction in E_d is owing to the low dispersion of drops in the presence of large drop diameters.

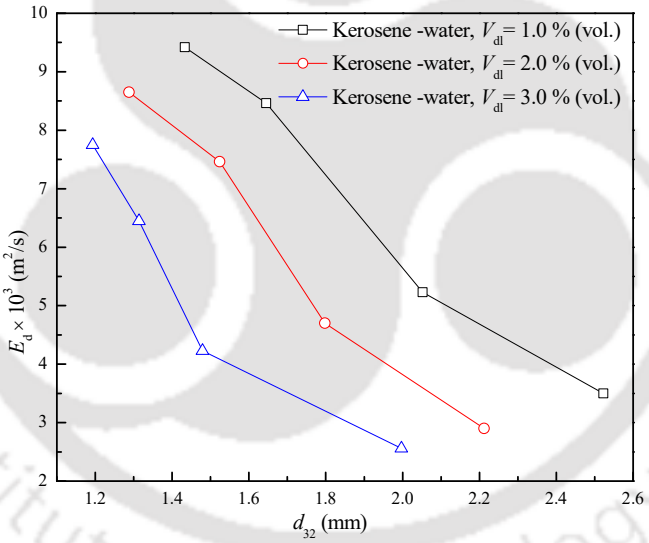

Figure 4.2. Effects of Sauter mean drop diameter on axial dispersion coefficient.

The E_d for a kerosene-water system at 1.0% volume was higher than the 2.0% and 3.0% dispersed phase volumes. The increase in the dispersed phase volume increases the system viscosity, which reduces the drop motion, and thus, the axial dispersion coefficient decreases. At V_{dl} = 1.0 % to 3.0% (vol. %) kerosene-water, the E_d decreases from 9.42 × 10^{-3} m^2/s (at d_{32} =1.43 mm) to 7.81 × 10^{-3} m^2/s (at d_{32} =1.19 mm), the reduction is 17.09%. Similarly, at V_{dl}: 1.0

% to 3.0% kerosene-water, the E_d decreases from 3.5 × 10^{-3} m^2/s (at d_{32} = 2.52 mm) to 2.56 × 10^{-3} m^2/s (at d_{32} =1.99 mm), the reduction is 26.85%. The typical values of drop diameter and their respective axial dispersion coefficients at experimental conditions are presented in Table 4.4.

4.4.2. Analysis of Residence Time Distribution

Typical results of the variation of the residence time distribution (RTD) at different jet velocities (u_j = 0.69 to 1.66 m/s) at V_{dl} = 1.0% vol. (paraffin) are shown in Fig. 4.5. When the tracer is injected, it moves downward and disperses down the column, and the tracer concentration in the column drops after reaching a peak for a length of time. For the different jet velocities, the mean residence times (t_m) are 27.74 s (at u_j = 0.69 m/s), 26.54 s (at u_j = 0.96 m/s), 24.25 s (at u_j = 1.38 m/s), and 23.73 s (at u_j = 1.66 m/s). The increase in the jet velocities leads to a reduction in the mean residence time of the system. The reduction in the mean residence time is due to the momentum impacted by the jet on the downward flowing liquid phase, resulting in shorter exit times.

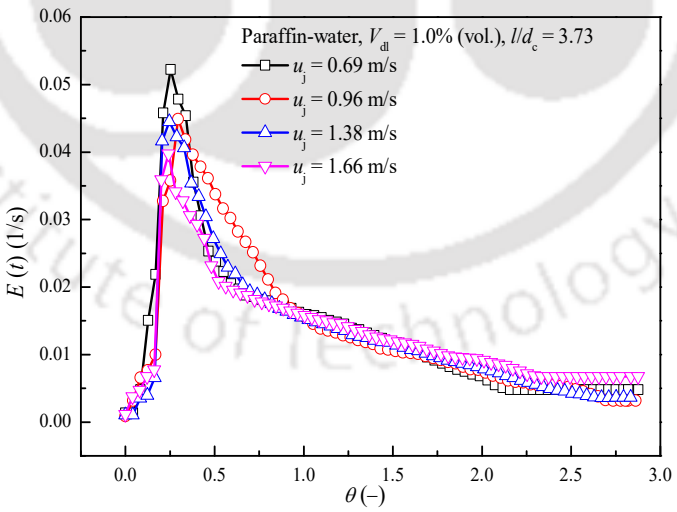

Figure 4.3. Typical RTD curve at different jet velocities.

4.4.3. Effect of Jet Velocity on Axial Dispersion Coefficient

The effect of liquid jet velocity (u_j = 0.69 to 1.66 m/s) on axial dispersion coefficient (E_d) for dispersed liquids (i.e., kerosene, diesel, 1-decanol, and paraffin) is shown in Fig. 4.6a to Fig. 4.6d. It is noticed that E_d increases with an increase in the liquid jet velocity for all the dispersed phases. The liquid jet velocity profoundly affects the mixing of dispersed phases inside the column. For the kerosene-water, an increase in the liquid jet velocity increases the turbulence of the system, which in turn increases the axial dispersion coefficient. As the jet velocity increases, the momentum transfer between the phases increases, causing scattering and dispersion of the drop. As a result, the axial dispersion coefficient increases. The smaller penetration length at minimum jet velocity (u_j = 0.69 m/s) is also due to the low momentum transfer. A similar observation of an increase in E_d with jet velocity for different dispersed phase liquids (diesel-water, 1-decanol-water, and paraffin-water). At the minimum velocity (u_j = 0.69 m/s), the kerosene-water (V_{dl}: 1.0% and 3.0%) E_d reduced from 3.5 $\times 10^{-3}$ m^2/s to 2.56 $\times 10^{-3}$ m^2/s, the reduction is 26.85% while at maximum jet velocity (u_j = 1.66 m/s), the E_d of kerosene-water (V_{dl} = 1.0% and 3.0%) is reduced from 9.42 $\times 10^{-3}$ m^2/s to 7.8 $\times 10^{-3}$ m^2/s, the reduction is 17.19%. For diesel-water (V_{dl} = 1.0% and 3.0%), the reduction of E_d is 25.61% (at u_j = 0.69 m/s), while at u_j = 1.66 m/s, the E_d reduced to 14.32%. Similarly, the E_d of 1-decanol-water (V_{dl} = 1.0% and 3.0%) was reduced to 24.60% (at u_j = 0.69 m/s) and 13.75% (at u_j = 1.66 m/s). In the case of Fig. 4.6d, the paraffin-water (V_{dl}: 1.0% and 3.0%) E_d was reduced to 21.95% (at u_j = 0.69 m/s) and 9.43% (at u_j = 1.66 m/s).

4.4.4. Effect of Dispersed Phase Volume on Axial Dispersion Coefficient

The order of the E_d for all the dispersed phase volume (V_{dl} = 1.0% to 3.0%) is E_d (paraffin) > E_d (1-decanol) > E_d (diesel) > E_d (kerosene). It is found that at constant jet velocity, the E_d

decreases with an increase in the dispersed phase volume. At a constant jet velocity, an increase in the viscosity of the dispersed phase volume decreases the liquid circulation in a column.

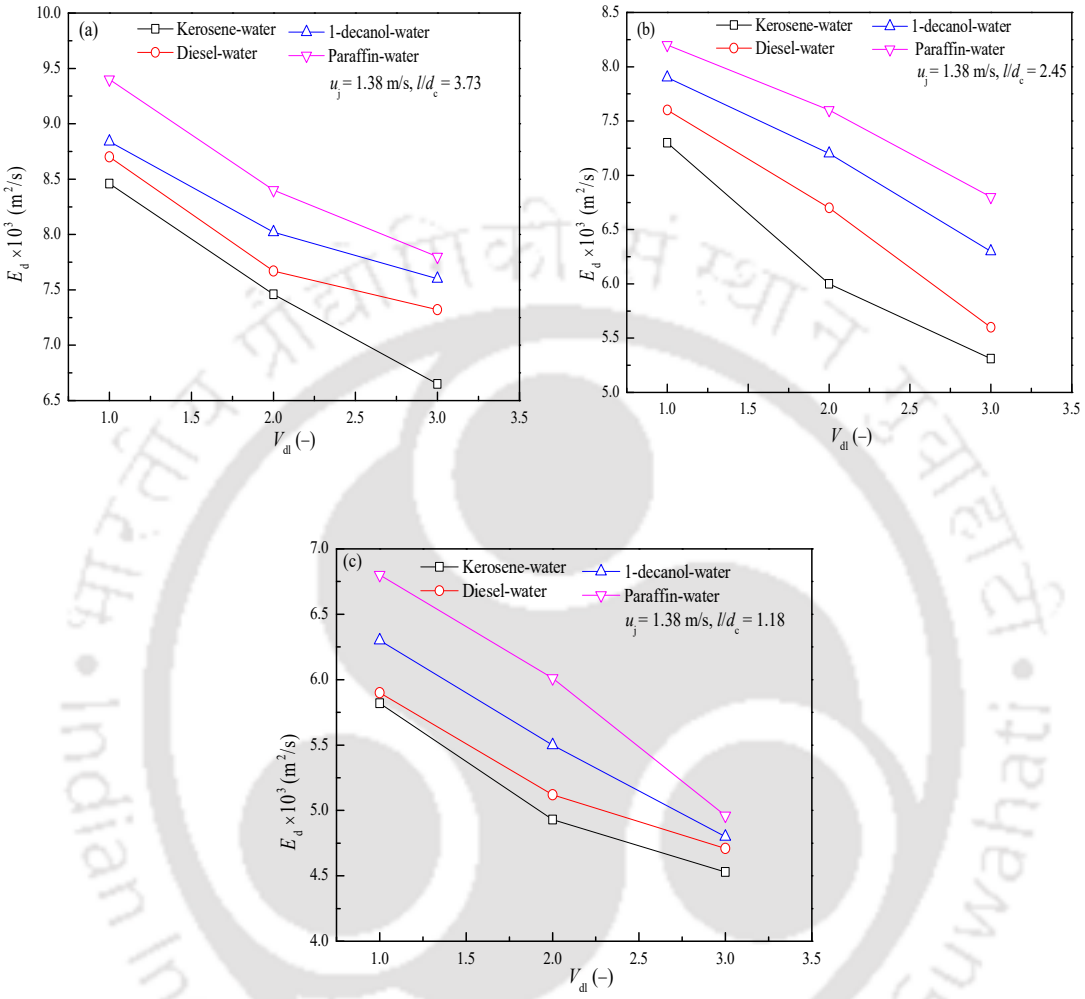

Figure 4.4. Effect of dispersed phase volume on axial dispersion coefficient as a function of different aspect ratios: (a) $l/d_c = 3.73$, (b) $l/d_c = 2.45$, and (c) $l/d_c = 1.18$.

This is because of an increase in the dispersed phase volume increases the system viscosity; as a result, the circulation inside the column decreases, which hinders the drop mobility. When the dispersed phase has a higher viscosity, the drag force in the dispersed droplet mixture increases. As a result, the axial dispersion coefficient in the system decreases. In Fig. 4.7a, E_d of kerosene-water (at $V_{dl} = 1.0\%$, $l/d_c = 3.73$) is 8.46×10^{-3} m^2/s, while the E_d of paraffin-water (at $l/d_c = 3.73$) is 9.4×10^{-3} m^2/s, the increment is about 11.11%. For 3.0% volume, the

increment is 17.29% as the system changes from kerosene-water to paraffin-water. Similarly, in the case of (at l/d_c = 2.45, V_{dl} = 1.0%), the E_d increases from 7.3 × 10^{-3} m^2/s to 8.2 × 10^{-3} m^2/s as it changes from kerosene-water to paraffin-water, the increment is 12.32% as shown in Fig. 4.7b. For l/d_c = 1.18 at a 1.0% volume of kerosene-water and paraffin-water, the increment of E_d is 16.83%, as presented in Fig. 4.7c. Therefore, at constant jet velocity, the influence of dispersed phase volume on axial dispersion coefficient is higher at l/d_c = 3.73 than at l/d_c = 2.45 and 1.18 at different dispersed phase volumes.

4.4.5. Effect of Aspect Ratio on Axial Dispersion Coefficient

The effect of aspect ratios (l/d_c= 3.73 to 1.18) on axial dispersion coefficient (E_d) at different jet velocity (u_j = 0.69 to 1.66 m/s) and different dispersed phase volume (V_{dl} = 1.0% to 3.0%) is shown in Fig. 4.8a to Fig. 4.8c. At minimum jet velocity (u_j = 0.69 m/s) and dispersed phase volume (V_{dl} =1.0%), it is observed that the maximum and minimum axial dispersion coefficients are at the aspect ratio of l/d_c = 3.73 and 1.18, respectively, as shown in Fig. 4.8a. A similar observation is shown in Fig. 4.8b and Fig. 4.8c. The jet penetration causes significant turbulence near l/d_c = 3.73, and the intensity of turbulence decreases as l/d_c approaches to 2.45 and 1.18. The collision of dispersed phase drops near the surface of the column is more intense, resulting in resistance to penetrate. It is observed that the maximum value of axial dispersion coefficient is noticed to be at probe 1 (which is near the tracer inlet location). In contrast, the minimum value is observed at probe 3 (which is near the bottom of the column). The existence of a jet penetration produces considerable turbulence, resulting in the highest axial dispersion coefficient at l/d_c = 3.73. The strong interaction between penetrating jets and dispersed phase drops causes high turbulence in this region. As l/d_c approaches 2.45 and 1.18, the degree of turbulence diminishes, and therefore the axial dispersion coefficient decreases. The penetration length of the jet in the present system approaches l/d_c = 3.73. Due to the resistance imposed by

dispersed phase drop, the magnitude of jet penetration length at a given jet velocity decreases when the aspect ratios are l/d_c = 2.45 and 1.18.

4.4.6. Development of an Empirical Correlation for Axial Dispersion Coefficient

An attempt has been made to predict the axial dispersion coefficient (E_d) by considering the various physical properties and operating and geometrical variables. The axial dispersion coefficient is influenced by the mixture density (ρ_{mix}), mixture viscosity (μ_{mix}), mixture surface tension (σ_{mix}), liquid jet velocity (u_j), axial height (l), column diameter (d_c), and acceleration due to gravity (g). The functionality of the axial dispersion coefficient can be expressed as

$$E_d = f\left(\rho_{mix}, \mu_{mix}, \sigma_{mix}, l, u_j, d_c, g\right) \tag{4.13}$$

From Buckingham's pi theorem and applying the multiple linear regression analysis, the relationship between the axial dispersion coefficient and the different dimensionless groups is expressed as

$$\frac{E_d}{d_c u_j} = 3.16\times10^{9}\left(\mathrm{Re}\right)^{-0.341}\left(We\right)^{-3.113}\left(Fr\right)^{3.426}\left(\frac{l}{d_c}\right)^{0.342} \tag{4.14}$$

where Re is the Reynolds number $\left(=\frac{d_c u_j \rho_{mix}}{\mu_{mix}}\right)$, We is the Weber number $\left(=\frac{u_j^2 d_c \rho_{mix}}{\sigma_{mix}}\right)$, and Fr is the Froude number $\left(=\frac{u_j^2}{g d_c}\right)$. The standard error and the correlation coefficient are found to be 0.08 and 0.98, respectively. Figure 4.9a shows the parity plot between experimental data and the predicted axial dispersion coefficients (Eq. 4.14).

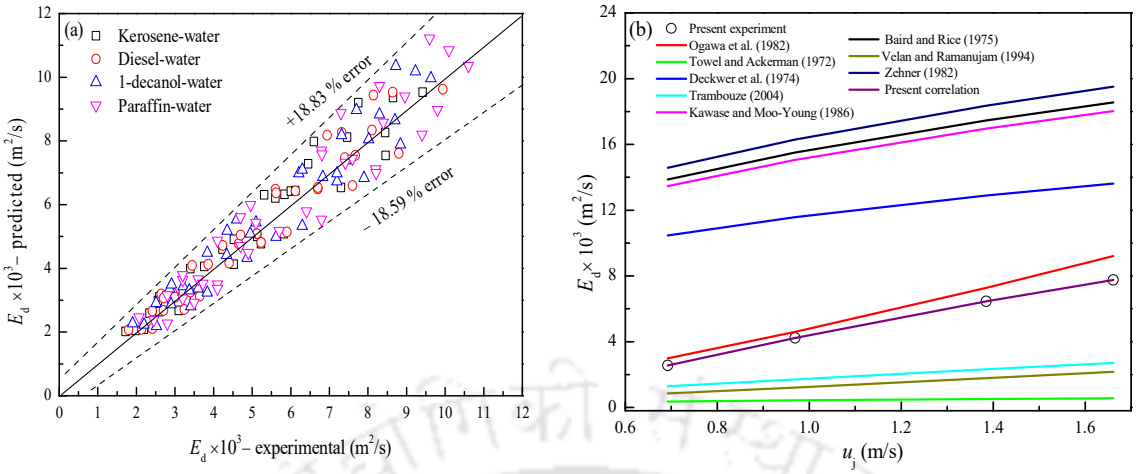

Figure 4.5. (a) Parity of experimental and predicted data of axial dispersion coefficient and (b) comparison of experimental data with the present correlation and other correlations.

The error between the experimental and predicted values is within the range of ± 18.83%. The correlation (Eq. 4.14) was valid for the ranges: $2.04 \times 10^4 \leq Re \leq 9.03 \times 10^4$; $3.73 \times 10^2 \leq We \leq 2.18 \times 10^3$; $0.889 \leq Fr \leq 5.116$. The present experimental data of E_d is compared with the developed correlation and other published correlations (Baird and Rice, 1975; Deckwer et al., 1974; Kawase and Moo-Young, 1986; Ogawa et al., 1982; Towell and Ackerman, 1972; Trambouze, 2004; Velan and Ramanujam, 1994; Zehner, 1982). A good agreement between the developed correlations and current experimental data is shown in Fig. 4.9b. The mean deviation (MD) and the root mean square deviation (RMSD) obtained from the present study were also compared with the other correlations and are presented in Table 4.5. It is observed that the experimental values of E_d with the developed correlations (Eq. 4.14), the MD was 10.01%. The compared correlations by Ogawa et al. (1982) (MD of 49.33%) and Trambouze (2004) (AARE of 58.25%) were found to be closed to the present experimental data. The correlations of Deckwer et al. (1974), Kawase and Moo-Young (1986), Baird and Rice (1975), and Zehner (1982) were found to be overpredicted with the current experimental data. In contrast, the correlations of Velan and Ramanujam (1994) and Towel and Ackerman (1972) were underpredicted. The deviations from the other correlations with the present experimental

data may be due to the different experimental conditions, such as physical and chemical properties, geometrical and operating variables.

Table 4.3. Comparison of experimental results with developed correlations and other correlations.

Authors	Mean deviation (MD) (%)	Root mean square deviation (RMSD) (%)
Ogawa et al. (1982)	49.33	63.93
Towel and Ackerman (1972)	90.13	94.06
Deckwer et al. (1974)	166.50	197.23
Trambouze (2004)	58.25	59.20
Kawase and Moo-Young (1986)	247.03	281.16
Baird and Rice (1975)	257.24	292.02
Velan and Ramanujam (1994)	74.96	74.96
Zehner (1982)	275.60	311.58
Present correlation	10.01	11.80

4.4.7. Estimation of Dispersion Due to Drop Motion (D_d) and Velocity Characteristic Factor (k)

The analysis of the axial dispersion coefficient is done by the velocity distribution model. The experimental value of the axial dispersion coefficient using the velocity distribution model is calculated by Eq. (4.10). The predicted value of the axial dispersion coefficient based on the velocity distribution can be obtained using Eq. (4.15)

$$E_{\mathrm{d,Pred}} = \frac{d_c^2 u_j^2}{k_{\mathrm{pred}} D_{\mathrm{pred}}} + D_{\mathrm{pred}} \tag{4.15}$$

where k_{pred} and D_{pred} are obtained using the developed correlations (shown in Table 4.6).

4.4.7.1. Effect of Dispersed Phase Volume on Dispersion Due to Drop Motion (D_d) and Velocity Characteristic Factor (k)

It is noticed that when the dispersed phase volume increases, the D_d decreases. This is because the viscosity of the system increases as the dispersed phase volume increases.

As a result, the hydrodynamic interaction between the dispersed and continuous phases increases, lowering the rate of drop collisions, and thus D_d decreases. Also, the increase in dispersed phase volume increases the shear stress between the continuous and dispersed phase mixture, thus reducing the drop mobility. The reduction in dispersion due to drop motion is 27.99% (for kerosene-water) as the dispersed phase volume changes from 1.0% to 3.0%. Similarly, the reduction is 28.31% for a paraffin-water system for the same range of changing the dispersed phase volume. The influence of dispersed phase volume on velocity characteristic factor (k) is shown in Fig. 4.10b. It is noticed that k increases as the dispersed phase volume increases. The increase in the dispersed phase volume increases the system viscosity while decreasing the turbulence and circulation of the phases in the column. The reduction in turbulence and the phase circulation improves the velocity characteristic factor.

4.5. Conclusions

The present study describes the mixing characteristics of liquid-liquid dispersion in a jet-driven mixing column. Mixing characteristic is enunciated in terms of the axial dispersion coefficient. The operating variables and the system's physical properties have a considerable influence on the axial dispersion coefficient. The axial dispersion coefficient increase as the jet velocity increases, but it decreases as the viscosity increases. The order of axial dispersion coefficient

in different dispersed phase liquids is E_d (paraffin) > E_d (1-decanol) > E_d (diesel) > E_d (kerosene). The axial dispersion coefficient is also analyzed by the velocity distribution model. A velocity distribution model parameter such as velocity characteristic factor increases, and dispersion due to drop motion decreases with the system viscosity. The axial dispersion coefficient was also interpreted using a mechanistic model based on the liquid exchange parameter between the downward and upward flow regimes and dispersion by phase circulation. The dispersion caused by the phase circulation was found to increase with the increase in the jet velocity. The proposed correlation of axial dispersion coefficient predicts the experimental value in the error range of ± 18.73%.

CHAPTER 5

EXTRACTION EFFICIENCY AND OVERALL MASS TRANSFER COEFFICIENT

Abstract

This chapter discussed the experimental study of the extraction efficiency and the overall mass transfer in a jet-driven liquid-liquid extraction column. The current study reports on the extraction efficiency, distribution coefficient, height of transfer unit, and overall mass transfer coefficient. The height of the transfer unit and the overall mass transfer coefficient based on the continuous phase are studied. The overall mass transfer coefficient (K_La) range was found to be 0.73 to 8.49 s^{-1} and 1.23 to 9.42 s^{-1}, respectively. A correlation is established based on the operating variables and physical parameters to predict the overall mass transfer coefficient.

5.1. Introduction

Over the past years, the interest in the recovery of carboxylic acids, such as acetic acid and propionic acid from wastewater have gained significant attention among the researchers (Piwowarek et al., 2021; Saha et al., 2000). There are numerous techniques available for industrial wastewater treatment, including chemical coagulation (Song et al., 2004), advanced oxidation process (Jiménez et al., 2019), and membrane separation process (Wódzki et al., 2000), etc. However, these processes involve high manufacturing costs, operational issues, high consumption of chemical agents, etc. Therefore, it will be an advantage to study using a jet-driven liquid-liquid extraction column which is economically effective.

The degree of mixing is an important parameter for the extraction of contaminants by treating immiscible liquids (Hosseinzadeh et al., 2017). A mechanical or non-mechanical mixer may

be used to mix immiscible liquids. One of the non-mechanical mixers that can be used for liquid-liquid extraction is the jet-driven extraction column. Jet columns have several advantages in many industrial research areas such as extraction, chemical reaction, sewage treatment, sludge treatment, and liquid metal transfer (Kirchner, 1974; Majumder, 2016; Ohkawa et al., 1987b). The kinetic energy produced from the jet is allowed to plunge over the immiscible liquid inside the column. As a result, it generates intense turbulence, increasing the interfacial area of the phases (Sangtam et al., 2021a). The mixing of liquids by a plunging jet can improve heat and mass transfer performance (Yadav et al., 2016).

Only a few research on carboxylic acid extraction from wastewater using a jet extraction column have been studied in recent years (Gao et al., 2016). Dehkordi (2002a) extracted copper ions using a nozzle jet, and the extraction efficiency was seven to eight times higher than the CSTR. The jet type extractors were also used for blending crude oil (Treybal, 1980), uranium and thorium extraction (Suresh et al., 2005), butyric acid, succinic acid, and toluene extraction (Gao et al., 2016; Saien et al., 2006; Saien and Moradi, 2012). At a fixed nozzle diameter in a jet column, the extraction efficiency of succinic acid in n-butanol improves while the total mass transfer drops (Nosratinia et al., 2010). Several investigations on liquid-liquid extraction columns have shown that the mass transfer phenomenon is an important issue when designing industrial columns. Different liquid-liquid extractions were performed using a jet mixer, and it was reported that jet-type devices significantly increase the mass transfer (Tamir, 1994). Various researchers have used different types of columns for liquid-liquid extraction, including Kühni column (Oliveira et al., 2008), rotating disc contactor (Asadollahzadeh et al., 2017; Wang et al., 2002), static mixer (Voulgaropoulos et al., 2019), and jet extraction column (Dehkordi, 2002b; Gao et al., 2016). The jet column outperforms other conventional columns because the high-speed impingement causes substantial turbulence to mix the phases. Van de Sande and Smith, (1975) used a plunging water system and studied the mass transfer at constant

nozzle diameter, jet length, and liquid velocity. They stated that the bubbles penetration height and the gas entrainment affect the total mass transfer coefficient. Table 5.1 summarizes overall mass transfer coefficient correlations for jet-type columns.

The current study examines the effects of continuous phases (acetic acid-water and propionic acid-water), dispersed phases (i.e., kerosene, diesel, 1-decanol, and paraffin), jet velocities, dispersed liquid volume, viscosity, and surface tension on extraction efficiency, the height of transfer unit, distribution coefficient, and overall mass transfer in the liquid-liquid system. A new correlation is developed for the prediction of an overall mass transfer coefficient.

5.2. Theory for Estimation of Extraction Efficiency and Mass Transfer Coefficient

The extraction efficiency ($E\%$) of solute in the dispersed phase can be calculated by the following expression (Harington and Hossain, 2008)

$$E\% = \frac{C_{cl,out} - C_{cl,in}}{C_{cl,in}} \tag{5.1}$$

where $C_{cl,out}$ and $C_{cl,in}$ are the inlet and outlet solute concentrations in the continuous phase. The extraction efficiencies are calculated based on the continuous phase concentration in terms of the overall mass transfer coefficient. The distribution coefficient (D) solute can be calculated as (Cai et al., 2001; Harington and Hossain, 2008)

$$D = \frac{C_{dl}}{C_{cl}} \tag{5.2}$$

where C_{dl}, and C_{cl} are the solute concentration in a dispersed and continuous phase, respectively.

The overall mass transfer coefficient is calculated using the number of transfer units and the column height, and it is denoted by (Lade et al., 2014)

$$h = HTU \times NTU \tag{5.3}$$

where

$$HTU = \frac{u_j}{K_L a} = \frac{h}{NTU_{cl}} \tag{5.4}$$

where NTU_{cl} is the number of transfer units for the continuous phase, $K_L a$ is the overall mass transfer coefficient (s^{-1}), u_j is the jet velocity (m/s), and h is the column height (m).

5.3. Experimental Setup, and Materials

5.3.1. Experimental Setup

The extraction and mass transfer study was performed based on the change of solute concentration of acetic acid and propionic acid in water. The solute concentration in the continuous phase was varied from 0.03 to 0.08 M, respectively. Figure 5.2 represent the liquid-liquid extraction process at different time.

The physical properties of the liquids are shown in Table 5.2. The dispersed phase volume and the jet velocity range were taken between 1.0% to 3.0% and 2.25 to 3.57 m/s, respectively. For each experimental run, the continuous phase inside the column was kept at a constant height of 0.29 m. A water coil was jacketed to maintain a consistent temperature around the column. Columns D_1, D_2, and D_3 show how the dispersed liquid behaves at various liquid jet velocities. Before collecting the outlet sample for each experiment, the continuous and dispersed phase systems were allowed to circulate continuously inside the column. The sample was then collected after every 4 minutes from the column outlet. The collected samples were transferred into a separating funnel, separated as organic and aqueous phases, and it was allowed to settle

for a certain time. After settling, 10 ml of the lower layer aqueous phase was collected into a conical flask and titrated with NaOH solution (0.1N) and phenolphthalein as the indicator.

5.3.2. Materials

The dispersed phases used were 1-decanol (with purity 98%) and paraffin liquid (with purity 98%) which were purchased from Sigma-Aldrich, Himedia Laboratories Pvt. Ltd, respectively. The other dispersed phases as kerosene and diesel were taken from a nearby gas station. The acetic acid (glacial with purity 100%) and propionic acid were purchased from Merck Pvt. Ltd and Himedia Laboratories Pvt. Ltd, respectively. The surface tension and viscosity of a dispersed liquid were measured by the Tensiometer (K9-MK1, KRUSS GmbH co., Germany) and Absolute viscometer (DV2TLVTJ0, BRK Instrument India LLP).

Table 5.1. Physical properties of the liquid at 273 K.

Liquid	Density (kg/m^3)	Surface tension (N/m)	Viscosity $\times 10^3$ (kg/m s)
Acetic acid	1045	0.027	1.155
Propionic acid	995	0.026	1.02
Water	998	0.071	1.00
Kerosene	810	0.034	1.56
Diesel	819	0.028	3.16
1-decanol	828	0.029	11.07
Paraffin liquid	840	0.026	21.07

5.4. Results and Discussion

5.4.1. Influence of Time on Solute Concentration

The influence of the different solute concentrations at different dispersed phases (kerosene, diesel, 1-decanol, and paraffin) with time is shown in Fig. 5.3a to Fig 5.3f. At constant (for u_j = 3.57 m/s, and V_{dl} = 3.0%), the solute concentration in the continuous phase was higher in the kerosene phase than in diesel, 1-decanol, and paraffin.

5.4.2. Effects of Jet Velocity on Extraction Efficiency

The experimental results show that the extraction efficiency (E%) increases with the jet velocity for all the dispersed phases. With an increase in the continuous phase flowrate, the jet momentum increases, which results in a higher dispersed droplet formation and thus increases the extraction efficiency.

5.4.2. Effect of Dispersed Phase Volume on Extraction Efficiency

The extraction efficiency for each dispersed phase (V_{dl} = 1.0% to 3.0%) is: E% (propionic acid-water-paraffin > acetic acid-water-paraffin) > E% (propionic acid-water-1-decanol > acetic acid-water-1-decanol) > E% (propionic acid-water-diesel > acetic acid-water-diesel) > (propionic acid-water-kerosene > acetic acid-water-kerosene). The experimental observation shows that the extraction efficiency increases at constant jet velocity as the dispersed volume phase increases from 1.0% to 3.0%.

5.4.3. Effect of Time on the Extraction Efficiency

In the present study, the sample was collected and measured after every 4 minutes for the extraction process. It was performed by constantly circulating the continuous and the dispersed phase mixture inside the column. The extraction efficiency is improved by increasing the continuous phase and the dispersed phase concentration. From the experimental results, the

extraction efficiency of acetic and propionic acid increased from 4 to 16 minutes, but the extraction time remains unchanged when it exceeds 20 minutes.

5.4.4. Distribution Coefficient for Solute Concentration

In the current study, the distribution coefficient decreased at low solute concentrations. The distribution coefficient is determined by solute concentration in the continuous and dispersed phases. The dispersed phase (paraffin) of acetic acid and propionic acid in water shows a higher distribution coefficient in the case of propionic acid (D = 0.951). As the initial solute concentrations increase, the distribution coefficient also increases with the dispersed phase volume. The distribution coefficients of acetic acid and propionic acid in different dispersed phases are listed in the following order: paraffin > 1-decanol > diesel > kerosene.

5.4.5. Effect of Jet Velocity and Solute Concentrations on HTU

The influence of the jet velocity and solute concentration on the height of transfer unit (HTU) is shown in Fig. 5.8a to Fig. 5.8d. It is seen that the HTU decreases with the increase in the jet velocities for all the dispersed phases. Initially, the HTU drops rapidly, and it starts to move slowly as the jet velocity increases. The HTU in kerosene systems is higher than in diesel, 1-decanol, or paraffin systems. The HTU decreases suddenly as the jet velocity rises from 2.25 to 2.96 m/s. However, beyond 2.96 m/s, the subsequent increases in jet velocity have little effect on the HTU. At a low jet velocity, the breakage of a dispersed droplet is insignificant, resulting in an increase in the HTU by lowering mass transfer efficiency.

5.4.9. Development of Correlation for Overall Mass Transfer Coefficient

The present study attempted to predict the $K_L a$ by considering the different physical properties, operating, and geometrical variables. The different variables, such as jet velocity, nozzle diameter, the density of the liquid mixture, the viscosity and surface tension of the liquid mixture, the acceleration due to gravity, and influenced the overall mass transfer coefficient.

All these relevant variables were used for developing the correlation. Overall mass transfer coefficient can be expressed as

$$\frac{K_L a\, d_c}{u_j} = 1.85\times10^{-9}\left(\mathrm{Re}\right)^{1.428}\left(We\right)^{-0.318}\left(Fr\right)^{0.129}\left(\frac{L_j}{d_c}\right)^{-1.973} \tag{5.12}$$

Equation (5.12) is valid for the range of $22.7839\times10^4 \le \mathrm{Re} \le 62.038\times10^3$, $34.546\times10^3 \le We \le 5.008\times10^3$, $260 \le Fr \le 104$, and $0.22 \le L_j / d_c \le 0.21$. The standard error and the correlation coefficient are 0.104 and 0.95, respectively.

5.5. Conclusions

This work describes an experimental investigation of the extraction efficiency and overall mass transfer coefficient in a liquid-liquid jet-driven extraction column. The liquids (kerosene, diesel, 1-decanol, and paraffin) were used as the dispersed phase, while acetic acid and propionic acid in water were used as the continuous phase. The impacts of the jet velocity, dispersed phase volume, and the physical properties of the system were studied. The experimental results showed that the performance of the jet-driven column for extraction improved as the jet velocity increased. As the jet velocity increases, the phase interaction between the mixture liquids increases, thus improving extraction efficiency. The extraction efficiency is improved by increasing the continuous phase and the dispersed phase concentration. The extraction efficiency range for acetic acid-water in all dispersed phases was 3.33% to 43.75%, while the extraction efficiency range for propionic acid was 6.66% to 48.75% for all the dispersed phases. The extraction efficiency improves as the distribution coefficient increases. The impact of jet velocity and solute concentration on transfer unit height was also investigated. The overall mass transfer coefficient appeared to be significantly influenced by the liquid jet velocity and dispersed phase volume. The overall mass transfer for acetic acid was found to be between 0.73 to 8.49 s^{-1}, and for propionic acid, it was 1.23 to 9.43

s^{-1}. In the present study, the overall mass transfer for propionic acid in paraffin was higher than that of acetic acid in paraffin. A general correlation for overall mass transfer has been developed based on the operating variables of the liquid-liquid jet-driven extraction column.

CHAPTER 6

OVERALL CONCLUSIONS AND FUTURE RECOMMENDATIONS

This particular chapter outlines the overall conclusions and future recommendations drawn from the present work using the jet-driven liquid-liquid extraction column.

6.1. Overall Conclusions

6.1.1. Liquid-liquid Entrainment Characteristics

- The experimental study on liquid-liquid entrainment is carried out using a jet-driven column.
- The experimental results show that increasing the dispersed phase volume enhances the rate of energy dissipation.
- The present experimental condition shows that the energy dissipation coefficient (K_m) drops at constant Reynolds numbers, resulting in a higher energy usage efficiency for mixing.
- The maximum penetration heights of kerosene, 1-decanol, paraffin, and soybean were found to be 0.70 m, 0.66 m, 0.65 m, and 0.63 m at the jet momentum of I = 0.31 kg m/s^2.
- The liquid penetration height is influenced by the liquid jet kinetic energy and the system properties. The liquid-liquid penetration height is correlated to the Reynolds number, Weber number, Froude number, and jet length.
- A mechanistic model based on the shell momentum balance method is developed and validated using the current experimental data. An empirical correlation is also proposed for predicting the penetration height based on the operating variables.

6.1.2. Drop Size Distribution and Drop Aspect Ratio

- The hydrodynamic characteristics study on drop size distribution, drop aspect ratio, and interfacial area in a jet-driven liquid-liquid extraction column were studied.
- Based on the experimental result, the drop size decreases with increased jet velocity and dispersed phase volume. Also, the drop size and its distribution depend on the system operations and physical properties.
- The log-logistic model fits the drop size distribution with the least error.
- The drop aspect ratio illustrates that as the jet velocity increases, the drop spherical reduces. The spherical drop size reduced as the dispersed phase volume increased.
- The range of the Sauter mean drop diameter is between 0.90 to 2.52 mm.
- The maximum interfacial area is 50.31 m^2/m^3 (paraffin-water), and the minimum is 6.040 m^2/m^3 (kerosene-water).
- The drop collision frequency increases due to an increase in the liquid jet momentum, resulting in the breakage of dispersed liquids into uniform small drop size.
- General correlations are developed based on the present experimental conditions for Sauter mean drop diameter, drop aspect ratio, distribution function parameters, and interfacial area.

6.1.3. Dispersion Characteristics and its Analysis

- The dispersion characteristics of liquid-liquid mixing were studied using a jet-driven mixing column.
- With increasing jet velocities, mean residence time drops. At different jet velocities, the mean residence times are 27.74 s (at u_j = 0.69 m/s), 26.54 s (at u_j = 0.96 m/s), 24.25 s (at u_j = 1.38 m/s), and 23.73 s (at u_j = 1.66 m/s), respectively.

- The axial dispersion coefficient (E_d) increases with jet velocity in the presence of all dispersed phases. The E_d reduces with increased dispersed phase volume at constant jet velocity.
- The axial dispersion coefficient is more influenced by the dispersed phase volume at the aspect ratio $l/d_c = 3.73$ than at $l/d_c = 2.45$ and $l/d_c = 1.18$.
- The range of the axial dispersion coefficient was found to be 25.6 to 106 cm^2/s.
- Estimation of dispersion due to drop motion, velocity distribution model, dispersion due to circulation, and turbulence were studied in different dispersed phases.
- The liquid exchange parameter (λ) increases with increasing dispersed phase volume while decreasing with increasing dispersed phase viscosity. A mechanistic model is derived based on the liquid exchange parameter between the upward and downward flow regimes and dispersion by phase circulation.
- An empirical correlation for axial dispersion coefficient based on operating, physical properties, and geometrical variables is developed. Also, a general correlation is proposed for velocity characteristics factor, dispersion due to drop motion, liquid exchange parameter, and dispersion by phase parameter based on the experimental data.

6.1.4. Extraction Efficiency and Overall Mass Transfer

- The experimental study was carried out for the extraction of acetic acid and propionic acid in water using dispersed phases such as kerosene, diesel, 1-decanol, and paraffin in a jet-driven liquid-liquid extraction column.
- The extraction efficiency is improved by increasing the continuous phase and the dispersed phase concentration.
- The extraction efficiency range for acetic acid-water was 3.33% to 43.75%, while the extraction efficiency range for propionic acid was 6.66% to 48.75% for all the dispersed phases.

- The impact of jet velocity and solute concentration on transfer unit height was also investigated.
- The overall mass transfer for acetic acid was found to be between 0.73 to 8.49 s^{-1}, and for propionic acid, it was 1.23 to 9.43 s^{-1}.
- A general correlation for overall mass transfer is developed based on the liquid-liquid jet-driven extraction column.

6.1.5. Future Recommendations

This work describes the hydrodynamics and mass transfer phenomena in a jet-driven liquid-liquid extraction column. The research includes liquid-liquid entrainment characteristics, drop size distribution, drop aspect ratio, mixing characteristics, extraction efficiency, and mass transfer coefficient. Additional research is still required to fully comprehend the scale and design of a jet-driven extraction column. The following are some of the potential future recommendations based on the present research works:

- The current study reports some detailed aspects of the liquid-liquid entrainment in the pilot lab-scale setup of the jet-driven column. It will be worthwhile to further study in higher operating conditions. This may provide higher liquid entrainment than the onset measure in the present study.
- Further studies on liquid entrainment can be carried out by adopting the CFD simulation method.
- The study should be further considered for the prediction of drop size distribution, drop aspect ratio, and interfacial area in a jet-driven column by a plunging liquid jet by CFD.
- Even though it is time-consuming, the photographic method has proven effective in measuring drop size in different regions. This approach measures the drop size at the column wall when there is enough light. The downside is that it cannot capture a proper

image at the center of the column due to limited visibility. The drop size at the center of the column can be measured using the probe technique, which is a faster method.

- The experimental work on axial dispersion is limited to a laboratory-scale column. This limits significant variations in liquid jet velocity, dispersed phase volume, and solute concentration. Therefore, studying the mixing characteristics in the scaleup column is recommended. The proposed mechanistic model may also be extended to analyze the dispersion caused by the circulation and turbulence in the scaleup process.
- The present work measured extraction efficiency by the physical extraction method. However, it is reported that deviations in results may be found by this method. Other methods, such as UV and HPCL can be used to measure the extraction of the solute phase from the continuous phase using different dispersed liquids. In the present study, the experiments were carried out at a lower range of solute concentration. It can be researched further from an industrial aspect by increasing the solute concentration.

NOMENCLATURE

Chapter 2

A, B, & C	Model parameter from Eq. (2.9) & Eq. (2.10)
a, b, c, & d	Constant parameters obtained from Eq. (2.5) & Eq. (2.31)
A_c	Area of the column (m^2)
a_j	Deceleration of jet penetration (m/s^2)
d_n	Diameter of the nozzle (m)
E_{sp}	Energy supplied (N m/s)
E_u	Energy utilized (N m/s)
F_z	Vertical force acting on the liquid jet (kgm/s^2)
H_p	Penetration height (m)
I	Momentum flow ($kg\ m/s^2$)
K_m	Coefficient for the loss of a mixing energy (–)
L_j	Length of the liquid jet (m)
l_n	Length of the nozzle (m)
$MARD$	Mean relative average deviation (–)
$\dot{m}_j$	Mass of liquid jet (kg/s)
N	Number of overall experimental data points (–)
$\Delta\dot{P}_{mom}$	Momentum pressure drop in a plunging liquid jet (N/m^2)
Q_j	Volumetric liquid jet flow rate (m^3/s)

$STDEV$	Standard deviation (–)
U	Standard uncertanity (–)
u_j	Velocity of the liquid jet (m/s)
u_{jc}	Velocity of the jet at the end of the penetration height (m/s)
u_{js}	Velocity of jet at the surface of the liquid pool (m/s)
u_l	Interstitial liquid velocity in the column (m/s)
U_r	Relative deviation (–)
u_{sl}	Superficial liquid velocity (m/s)
V_{cl}	Volumes of continuous liquid phase (m^3)
V_{dl}	Volume of dispersed liquid phase (m^3)
V_{min}	Minimum liquid jet velocity (m/s)
V_{tol}	Total volume of liquid mixture (m^3)
x_i	i^{th} component value of the experimental data (–)
$\overline{x}$	Mean of experimental data (–)

Greek letters

θ	The spread angle of the liquid core (degree)
ρ_m	Density of the liquid mixture (kg/m^3)
μ_m	Viscosity of liquid mixture (kg/m s)
σ_m	Surface tension of liquid mixture (N/m)
ρ_j	Density of liquid jet (kg/m^3)

ρ_{cl} continuous phase density (kg/m^3)

ρ_{dl} dispersed phase density (kg/m^3)

σ_{cl} continuous phase surface tension (N/m)

σ_{dl} dispersed phase surface tension (N/m)

μ_m mixture viscosity (kg/ms)

μ_{cl} continuous phase viscosity (kg/ms)

μ_{dl} dispersed phase viscosity (kg/ms)

ε_{dl} Volume fraction of dispersed liquid (–)

Δ Difference (–)

λ Constant parameter (–)

η_m Efficiency of energy utilization (–)

Nondimensional number

Re Reynolds number $\left(\frac{d_n u_j \rho_j}{\mu_j}\right)$ (–)

We Weber number $\left(\frac{\rho_m d_n u_j^2}{\sigma_j}\right)$ (–)

Fr Froude number $\left(\frac{u_j^2}{g d_n}\right)$ (–)

Ri Richardson number $\left(\frac{g \rho_m d_n}{\rho_j u_j^2}\right)$ (–)

Chapter 3

a, & b	Constant parameters obtained from Eq. (3.4)
A (j, k)	The Beta distribution function (–)
a_i	Interfacial area (m^2/m^3)
AARD	Average absolute relative deviation (–)
AR	Aspect ratio (–)
C	Column (–)
CDF	Cumulative distribution function (–)
d_{32}	Sauter mean drop diameter (m)
d_c	Diameter of column (m)
d_d	Drop diameter liquid (m)
d_{eq}	Equivalent drop diameter (m)
d_n	Diameter of nozzle (m)
DSD	Drop size distribution (–)
$F(d_d)$	Drop distribution function (–)
g	Acceleration due to gravity (m/s^2)
j	Lower shape parameter (–)
k	Upper shape parameter (–)
l_{maj}	Length of the major drop axis (m)

l_{min}	Length of the minor drop axis (m)
n_i	Number of drop size of diameter d_d (–)
P	Pressure (1 atm)
RF	Relative frequency (–)
RSD	Relative standard deviation (–)
T	Temperature (K)
u_j	Jet velocity (m/s)
u_t	Terminal velocity (m/s)
V_{cl}	Volume of continuous liquid (m^3)
V_{dl}	Volume of dispersed liquid (m^3)
V_{tol}	Total volume of liquid mixture (m^3)
w	Minimum value of d_d (m)
z	Maximum value of d_d (m)

Greek letters

ρ_m	Density of liquid mixture (kg/m^3)
μ_m	Viscosity of liquid mixture (kg/m s)
σ_m	Surface tension of liquid mixture (N/m)
λ	Ratio of equivalent drop diameter and the column diameter (–)
ψ	Aspect ratio (–)

ω	Constant parameter (–)
α	Drop shape parameter (–)
β	Scale parameter (–)
ε_{dl}	Volume fraction of dispersed liquid (–)

Non-dimensionless number

Eo	Eötövs number $\left(\frac{g\left(\rho_l-\rho_{dl}\right)d_{eq}^2}{\sigma_l}\right)$ (–)
Mo	Morton number $\left(\frac{g\left(\rho_l-\rho_{dl}\right)\mu_l^4}{\rho_l^2\sigma^3}\right)$ (–)
Ta	Tadaki number $\left(\mathrm{Re}_d\, Mo^{0.23}\right)$ (–)
Re_j	Reynolds number $\left(\frac{u_j d_d \rho_m}{\mu_m}\right)$ (–)
Re_d	Reynolds number $\left(\frac{d_n u_t d_{eq}}{\mu_l}\right)$ (–)
We	Weber number $\left(\frac{d_n u_j^2 \rho_m}{\sigma_m}\right)$ (–)

Chapter 4

a_{df}	Column cross section-area of downward flow (m^2)
a_{uf}	Column cross section-area of upward flow (m^2)
A to *C*	Coefficient constants (–)
AARE	Average absolute relative error (%)

C	Concentration of tracer solution (kg/m^3)
C_θ	Dimensionless tracer concentration (–)
C_0	Initial tracer concentration (kg/m^3)
$\overline{C}$	Average tracer concentration (kg/m^3)
C_{df}	Concentration of downward flow (kg/m^3)
C_{uf}	Concentration of upward flow (kg/m^3)
D_s	Molecular diffusivities (m^2/s)
D_d	Dispersion due to drop motion (m^2/s)
d_c	Column diameter (m)
d_n	Nozzle diameter (m)
d_{32}	Sauter mean drop diameter (m)
E_d	Axial dispersion coefficient (m^2/s)
$E\ (t)$	Exit age distribution time (1/s)
E_{df}	Axial dispersion of downward flow (m^2/s)
E_{uf}	Axial dispersion of upward flow (m^2/s)
E_{tr}	Dispersion caused by liquid-liquid turbulence (m^2/s)
E_{cr}	Dispersion caused by liquid-liquid circulation (m^2/s)
g	Acceleration due to gravity (m/s^2)
H	Height of the column (m)
K_c	Conductivity of solution (mS/cm)

K_w	Conductivity of water (mS/cm)
k	Velocity characteristic factor (–)
l	Distance between the tracer inlet and the detector point (m)
l_c	Length of column (m)
l_n	Length of nozzle (m)
N	Total number of experimental data (–)
Pe	Peclet number (–)
p	Coefficient in Eq. (4.28) (–)
STDEV	Standard deviation (–)
t_m	Mean residence time (s)
u_j	Jet velocity (m/s)
U	Standard uncertainty (–)
U_r	Relative uncertainty (–)
V	Volume of the column (ml)
V_{cl}	Continuous phase volume (m^3)
V_{dl}	Dispersed phase volume (%)
W	Circumference between downward flow and upward flow (m)
$\overline{x}$	Mean of experimental values (–)
x_i	i^{th} experimental value (–)

y	Slope of the Eq. (4.12) (–)
z	Dimensionless distance of probe from the tracer inlet (–)

Greek letters

ρ_m	Density of liquid mixture (kg/m^3)
μ_m	Viscosity of liquid mixture (kg/m s)
σ_m	Surface tension of liquid mixture (N/m)
σ_θ^2	Dimensionless variance function (–)
θ	Dimensionless time (–)
σ^2	Variance of RTD curve (–)
λ	Liquid exchange parameter (m/s)
δ	Parameter from Eq. (4.26) (–)

Chapter 5

AARE	Average absolute relative error (%)
C_{cl}^*	Equilibrium concentration of solute in continuous phase (mol.L^{-1})
C_{cl}	Solute concentration in continuous phase (mol.L^{-1})
$C_{cl,\,in}$	Solute concentration in the inlet and outlet continuous phase (mol.L^{-1})
$C_{cl,out}$	Solute concentration in the outlet and outlet continuous phase (mol.L^{-1})
C_{dl}	Solute concentration in dispersed phase (mol.L^{-1})

$C_{dl,\ in}$	Solute concentration in the inlet dispersed phase (mol.L^{-1})
$C_{dl,\ out}$	Solute concentration in the outlet dispersed phase (mol.L^{-1})
D	Distribution coefficient (–)
d_{32}	Sauter mean drop diameter (mm)
d_c	Column diameter (m)
d_n	Nozzle diameter (m)
E%	Extraction efficiency (–)
g	Acceleration due to gravity (m/s^2)
h	Column height (m)
HTU	Height of transfer unit based on continuous phase (m)
K_La	Overall mass transfer coefficient (s^{-1})
l_c	Length of column (m)
l_n	Length of nozzle (m)
L_j	Length of jet (m)
m	Equilibrium constant (–)
NTU_{cl}	Number of transfer unit based on continuous phase (m)
u_j	Jet velocity (m/s)
V_{cl}	Continuous phase volume (m^3)
V_{dl}	Dispersed phase volume (%)

GREEK LETTERS

θ	Jet angle (–)
ρ_m	mixture density (kg/m^3)
σ_m	mixture surface tension (N/m)
μ_m	mixture viscosity (kg/ms)

APPENDIX 1

Uncertainty Analysis

The present experiment was performed four times consecutively and the sum of all the readings was considered as the final value. The mean $(\bar{x})$ experimental data is expressed as

$$\bar{x} = \frac{1}{N}\sum_{i=1}^{N} x_i \tag{A1}$$

where x_i is the i^{th} experiment value and N represents the total number of experimental data. The standard uncertainty (U)for an experiment is calculated as

$$U = \frac{STDEV}{\sqrt{N}} \tag{A2}$$

The relative uncertainty (U_r) is estimated as

$$U_r = \frac{U}{\bar{x}} \times 100 \tag{A3}$$

The standard deviation is expressed as

$$STDEV = \sqrt{\frac{\sum_{1}^{N}\left(x_i - \bar{x}\right)^2}{N-1}} \tag{A4}$$

where $\bar{x}$ is the mean of experimental quantities.

APPENDIX 2

Procedure for Calculating Typical Multiple Regression

The regression equation is

$$d_{32}=\mathrm{d}_1\left(d_n\right)^{c_1}\left(\mathrm{Re}\right)^{c_2}\left(We\right)^{c_3} \quad \text{I}$$

Taking logarithm on both side of the Eq. (I)

$$\log\left(d_{32}\right)=\log(D_1)+C_1\log\left(d_n\right)+C_2\log\left(\mathrm{Re}\right)+C_3\log\left(We\right) \quad \text{II}$$

Eq. (II) can be written as

$$X=c_0+c_1Y_1+c_2Y_2+c_3Y_3+e \quad \text{III}$$

where $X=\log\left(d_{32}\right), X_1=\log\left(d_n\right), X_2=\log\left(\mathrm{Re}\right), X_3=\log\left(We\right)$ and $c_0=\log\left(d_1\right)$. The error term, denoted by e, must be minimized in order to estimate the regression model as follows:

$$\hat{X}=c_0+cY_3 \quad \text{IV}$$

where $\hat{X}$ denotes the predicted value of X

The intercept c_0 and the coefficients $c_1, c_2,$ and c_3 have been measured by multiple regression analysis using "Data Analysis Tool" of Software "Microsoft Excel"

The following calculation is used by the software to obtain the outputs.

Eq. (III) is expressed in matrix form for n $\left(\text{here } n=48\right)$ and $\left(\text{here } k=3\right)$ variables as

$$\begin{bmatrix} X_1 \\ X_2 \\ . \\ . \\ X_n \end{bmatrix} = \begin{bmatrix} 1\ Y_{11}\ Y_{12}\ .....Y_{1k} \\ 1\ Y_{21}\ Y_{22}.....Y_{2k} \\ . \\ . \\ 1\ Y_{n1}\ Y_{n1}.....Y_{nk} \end{bmatrix} \times \begin{bmatrix} c_1 \\ c_2 \\ . \\ . \\ c_n \end{bmatrix} + \begin{bmatrix} e_1 \\ e_2 \\ . \\ . \\ e_n \end{bmatrix} \quad \text{(V)}$$

$$X = Y \times C + e$$

Regression statistics

		Description
Multiple R	0.944	R = square root of R^2
R Square	0.890	R^2 = coefficient of determination
Adjusted R square	0.885	Adjusted R^2 used if more than one Y varaibles
Standard error	0.084	estimate of the st. dev. of the error e
Observations	48	Number of observations used in the regression (n)

Analysis of variance

	Degree of freedom	Sum of square	Mean of square	F-stat
Regression	2	2.615	1.307	183.273
Residual	45	0.326	0.0071	
Total	47	2.936		

Regression sum of square $= C'Y'X - n\bar{X}^2$

A total sum of square $= X'X - n\bar{X}^2$

Residual sum of square = Total sum of square − Regression sum of square

$$R^2 = \frac{\text{Regression sum of square}}{\text{Residual sum of square}}$$

$$F - stat = \frac{R^2/(k-1)}{(1-R^2)/(n-k)}$$

$$\text{Adjusted } R^2 = 1-(1-R^2)\left(\frac{n-1}{n-k}\right)$$

Standard error = $\sqrt{\frac{\text{Residual sum of square}}{n-k}}$

$X' = \begin{bmatrix} X_1 & X_2 & \cdots & X_n \end{bmatrix}$

$C' = \begin{bmatrix} C_1 & C_2 & \cdots & C_n \end{bmatrix}$

The F-stat is used to calculate the overall F-test for the null hypothesis $H_0 = c_i = 0$. The F-stat determines the corresponding Probability-value. The null hypothesis for the goodness fit is not rejected because it is greater than 0.05 at the 5% significance level.

References

Acharya, A., Mashelkar, R.A., Ulbrecht, J., 1977. Mechanics of bubble motion and deformation in non-Newtonian media. Chemical Engineering Science 32, 863–872. https://doi.org/10.1016/0009-2509(77)80072-9

Alban, F.B., Sajjadi, S., Yianneskis, M., 2004. Dynamic tracking of fast liquid-liquid dispersion processes with a real-time in-situ optical technique. Chemical Engineering Research and Design 82, 1054–1060. https://doi.org/10.1205/0263876041580631

Amani, P., Amani, M., Saidur, R., Yan, W.-M., 2017. Hydrodynamic performance of a pulsed extraction column containing ZnO nanoparticles: Drop size and size distribution. Chemical Engineering Research and Design 121, 275–286. https://doi.org/10.1016/j.cherd.2017.03.017

Amiri, T.Y., Moghaddas, J.S., Moghaddas, Y., 2011. A jet mixing study in two phase gas-liquid systems. Chemical Engineering Research and Design 89, 352–366. https://doi.org/10.1016/j.cherd.2010.06.009

Angle, C.W., Dabros, T., Hamza, H.A., 2006. Predicting sizes of toluene-diluted heavy oil emulsions in turbulent flow. Part 1-Application of two adsorption kinetic models for σE in two size predictive models. Chemical Engineering Science 61, 7309–7324. https://doi.org/10.1016/j.ces.2006.08.032

Angle, C.W., Hamza, H.A., 2006. Predicting the sizes of toluene-diluted heavy oil emulsions in turbulent flow Part 2: Hinze-Kolmogorov based model adapted for increased oil fractions and energy dissipation in a stirred tank. Chemical Engineering Science 61, 7325–7335. https://doi.org/10.1016/j.ces.2006.01.014

Aoyama, S., Hayashi, K., Hosokawa, S., Tomiyama, A., 2018. Shapes of single bubbles in

infinite stagnant liquids contaminated with surfactant. Experimental Thermal and Fluid Science 96, 460–469. https://doi.org/10.1016/j.expthermflusci.2018.03.015

Aoyama, S., Hayashi, K., Hosokawa, S., Tomiyama, A., 2016. Shapes of ellipsoidal bubbles in infinite stagnant liquids. International Journal of Multiphase Flow 79, 23–30. https://doi.org/10.1016/j.ijmultiphaseflow.2015.10.003

Aris, R., 1956. On the dispersion of a solute in a fluid flowing through a tube. Proceedings of the Royal Society of London. Series A. Mathematical and Physical Sciences 235, 67–77. https://doi.org/10.1098/rspa.1956.0065

Asadollahzadeh, M., Hemmati, A., Torab-Mostaedi, M., Shirvani, M., Ghaemi, A., Mohsenzadeh, Z.S., 2017. Use of axial dispersion model for determination of Sherwood number and mass transfer coefficients in a perforated rotating disc contactor. Chinese Journal of Chemical Engineering 25, 53–61. https://doi.org/10.1016/j.cjche.2016.06.007

Asadollahzadeh, M., Torab-Mostaedi, M., Shahhosseini, S., Ghaemi, A., 2016. Experimental investigation of dispersed phase holdup and flooding characteristics in a multistage column extractor. Chemical Engineering Research and Design 105, 177–187. https://doi.org/10.1016/j.cherd.2015.11.019

Asadollahzadeh, M., Torab-Mostaedi, M., Shahhosseini, S., Ghaemi, A., 2015. Using maximum entropy approach for prediction of drop size distribution in a pilot plant multi-impeller extraction contactor. RSC Advances 5, 95967–95980. https://doi.org/10.1039/C5RA18385E

Asai, S., Hatanaka, J., Maeda, H., 1988. Mass transfer in a liquid-liquid jet with cocurrent laminar flow. Chemical Engineering Science 43, 713–718. https://doi.org/10.1016/0009-2509(88)87030-1

Ayass, W.W., Nasir, E.F., Farooq, A., Sarathy, S.M., 2016. Mixing-structure relationship in jet-stirred reactors. Chemical Engineering Research and Design 111, 461–464. https://doi.org/10.1016/j.cherd.2016.05.016

Baird, M.H.I., Rice, R.G., 1975. Axial dispersion in large unbaffled columns. The Chemical Engineering Journal 9, 171–174. https://doi.org/10.1016/0300-9467(75)80010-4

Baldyga, J., Bourne, J.R., 1993. Drop breakup and intermittent turbulence. Journal of Chemical Engineering of Japan 26, 738-741. https://doi.org/10.1252/jcej.26.738

Baldyga, J., Bourne, J.R., Gholap, R. V, 1995. The influence of viscosity on mixing in jet reactors. Chemical Engineering Science 50, 1877–1880. https://doi.org/10.1016/0009-2509(95)00049-B

Berna, C., Escrivá, A., Muñoz-Cobo, J.L., Herranz, L.E., 2015. Review of droplet entrainment in annular flow: Characterization of the entrained droplets. Progress in Nuclear Energy 79, 64–86. https://doi.org/10.1016/j.pnucene.2014.11.011

Bertola, N., Wang, H., Chanson, H., 2018. A physical study of air-water flow in planar plunging water jet with large inflow distance. International Journal of Multiphase Flow 100, 155–171. https://doi.org/org/10.1016/j.ijmultiphaseflow.2017.12.015

Besagni, G., Deen, N.G., 2020. Aspect ratio of bubbles in different liquid media: A novel correlation. Chemical Engineering Science 215, 115383. https://doi.org/10.1016/j.ces.2019.115383

Besagni, G., Inzoli, F., 2019. Bubble sizes and shapes in a counter-current bubble column with pure and binary liquid phases. Flow Measurement and Instrumentation 67, 55–82. https://doi.org/10.1016/j.flowmeasinst.2019.04.008

Besagni, G., Inzoli, F., 2017. The effect of electrolyte concentration on counter-current gas-

liquid bubble column fluid dynamics: Gas holdup, flow regime transition and bubble size distributions. Chemical Engineering Research and Design 118, 170–193. https://doi.org/10.1016/j.cherd.2016.12.012

Besagni, G., Inzoli, F., 2016. Bubble size distributions and shapes in annular gap bubble column. Experimental Thermal and Fluid Science 74, 27–48. https://doi.org/10.1016/j.expthermflusci.2015.11.020

Besagni, G., Inzoli, F., De Guido, G., Pellegrini, L.A., 2016. Experimental investigation on the influence of ethanol on bubble column hydrodynamics. Chemical Engineering Research and Design 112, 1–15. https://doi.org/10.1016/j.cherd.2016.06.009

Bhaga, D., Weber, M.E., 1981. Bubbles in viscous liquids: shapes, wakes and velocities. Journal of Fuid Mechanics 105, 61–85. https://doi.org/10.1017/S002211208100311X

Bhattacharya, S., Kresta, S.M., 2004. Surface feed with minimum by-product formation for competitive reactions. Chemical Engineering Research and Design 82, 1153–1160. https://doi.org/10.1205/cerd.82.9.1153.44173

Bińi, A.K., 1993. Gas entrainment by plunging liquid jets. Chemical Engineering Science 48, 3585–3630. https://doi.org/10.1016/0009-2509(93)81019-R

Bin, A.K., Smith, J.M., 1982. Mass transfer in a plunging liquid jet absorber. Chemical Engineering Communications 15, 367–383. https://doi.org/org/10.1080/00986448208911082

Bonsignore, D., Volpicelli, G., Campanile, A., Santoro, L., Valentino, R., 1985. Mass transfer in plunging jet absorbers. Chemical Engineering and Processing: Process Intensification 19, 85–94. https://doi.org/10.1016/0255-2701(85)80007-6

Burgess, J.M., Molloy, N.A., McCarthy, M.J., 1972. A note of the plunging liquid jet reactor.

Chemical Engineering Science 27, 442–445. https://doi.org/10.1016/0009-2509(72)85082-6

Cai, W., Zhu, S., Piao, X., 2001. Extraction equilibria of formic and acetic acids from aqueous solution by phosphate-containing extractants. Journal of Chemical and Engineering Data 46, 1472–1475. https://doi.org/10.1021/je010117i

Chatzi, E.G., Boutris, C.J., Kiparissides, C., 1991. On-line monitoring of drop size distributions in agitated vessels. 1. Effects of temperature and impeller speed. Industrial & Engineering Chemistry Research 30, 536–543. https://doi.org/10.1021/ie00051a015

Chenwei, W., Ming zhong, L., Chen, L., Weiyang, L.W., 2013. Measurement and analysis of bimodal drop size distribution in a rotor-stator homogenizer. Chemical Engineering Science 102, 622–631. https://doi.org/10.1016/j.ces.2013.08.030

Clift, R., Grace, J.R., Weber, M.E., 1978. Bubbles, drops, and particles. Academic Press, New York.

Cumming, I.W., 1975. The impact of falling liquids with liquid surfaces. P.h.D Thesis, Loughborough University of Technology.

Danckwerts, P. V, 1953. Continuous flow systems: distribution of residence times. Chemical Engineering Science 2, 1–13. https://doi.org/10.1016/0009-2509(53)80001-1

De Hert, S.C., Rodgers, T.L., 2017. On the effect of dispersed phase viscosity and mean residence time on the droplet size distribution for high-shear mixers. Chemical Engineering Science 172, 423–433. https://doi.org/10.1016/j.ces.2017.07.002

Deckwer, W.-D., Burckhart, R., Zoll, G., 1974. Mixing and mass transfer in tall bubble columns. Chemical Engineering Science 29, 2177–2188. https://doi.org/10.1016/0009-2509(74)80025-4

Dehkordi, A.M., 2002a. Experimental investigation of an air-operated two-impinging-streams reactor for copper extraction processes. Industrial & Engineering Chemistry Research 41, 2512–2520. https://doi.org/10.1021/ie010508q

Dehkordi, A.M., 2002b. Liquid-liquid extraction with chemical reaction in a novel impinging-jets reactor. AIChE Journal 48, 2230–2239. https://doi.org/10.1002/aic.690481013

Dehkordi, A.M., 2002c. Application of a novel-opposed-jets contacting device in liquid-liquid extraction. Chemical Engineering and Processing: Process Intensification 41, 251–258. https://doi.org/10.1016/S0255-2701(01)00141-6

Dehkordi, A.M., 2001. Novel type of impinging streams contactor for liquid-liquid extraction. Industrial & Engineering Chemistry Research 40, 681–688. https://doi.org/10.1021/ie000279s

Deswal, S., Verma, D.V.S., 2007. Air-water oxygen transfer with multiple plunging jets. Water Quality Research Journal 42, 295–302. https://doi.org/10.1080/00986448808940437

Dhindsa, A., Wanchoo, R.K., Toor, A.P., 2020. Motion of nanofluid droplets through immiscible quiescent liquid: An experimental study. Industrial & Engineering Chemistry Research 59, 6247–6257. https://doi.org/10.1021/acs.iecr.9b06101

Eastwood, C.D., Armi, L., Lasheras, J.C., 2004. The breakup of immiscible fluids in turbulent flows. Journal of Fluid Mechanics 502, 309–333. https://doi.org/10.1017/S0022112003007730

Eggers, J., Villermaux, E., 2008. Physics of liquid jets. Reports on Progress in Physics 71. https://doi.org/10.1088/0034-4885/71/3/036601

El Hammoumi, M., Achard, J.L., Davoust, L., 2002. Measurements of air entrainment by vertical plunging liquid jets. Experiments in Fluids 32, 624–638.

https://doi.org/10.1007/s00348-001-0388-1

Emami, A., Briens, C., 2008. Study of downward gas jets into a liquid. AIChE journal 54, 2269–2280. https://doi.org/org/10.1002/aic.11524

Esmaeeli, B., Ghaemi, A., Shirvani, M., Hosseinzadeh, M., 2020. Mass transfer coefficient in the eductor liquid-liquid extraction column. Chinese Journal of Chemical Engineering (In Press). https://doi.org/10.1016/j.cjche.2020.12.017

Evans, G.M., Machniewski, P.M., 1999. Mass transfer in a confined plunging liquid jet bubble column. Chemical Engineering Science 54, 4981–4990. https://doi.org/10.1016/S0009-2509(99)00221-3

Fogler, H.S., 2016. Elements of Chemical Reaction Engineering, Fifth. ed. Pearson Education.

Fosberg, T.M., Heideger, W.J., 1967. Interphase mass transfer in binary liquid systems-Laminar liquid jets. The Canadian Journal of Chemical Engineering 45, 82–89. https://doi.org/10.1002/cjce.5450450205

Friedman, P.D., Katz, J., 1999. The flow and mixing mechanisms caused by the impingement of an immiscible interface with a vertical jet. Physics of Fluids 11, 2598–2606. https://doi.org/org/10.1063/1.870122

Funatsu, K., Hsu, Y.-C., Noda, M., Sugawa, S., 1988. Oxygen transfer in the water-jet vessel. Chemical Engineering Communications 73, 121–139. https://doi.org/10.1080/00986448808940437

Gao, Z., Zhao, M., Yu, Y., Li, Z., Han, J., 2016. Investigation of extraction fraction in confined impinging jet reactors for tri-butyl-phosphate extracting butyric acid process. Chinese Journal of Chemical Engineering 24, 310–316. https://doi.org/10.1016/j.cjche.2015.12.005

Gholam Samani, M., Haghighi Asl, A., Safdari, J., Torab-Mostaedi, M., 2012. Drop size distribution and mean drop size in a pulsed packed extraction column. Chemical Engineering Research and Design 90, 2148–2154. https://doi.org/10.1016/j.cherd.2012.06.002

Gliński, J., 2003. Determination of the conditional association constants from the sound velocity data in binary liquid mixtures. The Journal of Chemical Physics 118, 2301–2307. https://doi.org/10.1063/1.1534579

Godfrey, J.C., Slater, M.J., 1994. Liquid-liquid extraction equipment. Wiley New York.

Goshika, B.K., Majumder, S.K., 2019. Dispersion of liquid-liquid phase by a jet-induced gas-liquid-liquid mixing column developed for separation of organic pollutants. Separation Science and Technology 54, 535–548. https://doi.org/org/10.1080/01496395.2018.1504796

Goshika, B.K., Majumder, S.K., 2018. Entrainment and holdup of gas-liquid-liquid dispersion in a downflow gas-liquid-liquid contactor. Chemical Engineering and Processing: Process Intensification 125, 112–123. https://doi.org/10.1016/j.cep.2018.01.011

Greaves, D., Boxall, J., Mulligan, J., Montesi, A., Creek, J., Sloan, E.D., Koh, C.A., 2008. Measuring the particle size of a known distribution using the focused beam reflectance measurement technique. Chemical Engineering Science 63, 5410–5419. https://doi.org/10.1016/j.ces.2008.07.023

Harington, T., Hossain, M.M., 2008. Extraction of lactic acid into sunflower oil and its recovery into an aqueous solution. Desalination 218, 287–296. https://doi.org/10.1016/j.desal.2007.02.024

Hemmati, A., Torab-Mostaedi, M., Shirvani, M., Ghaemi, A., 2015. A study of drop size

distribution and mean drop size in a perforated rotating disc contactor (PRDC). Chemical Engineering Research and Design 96, 54–62. https://doi.org/10.1016/j.cherd.2015.02.005

Hernandez-Alvarado, F., Kalaga, D. V., Turney, D., Banerjee, S., Joshi, J.B., Kawaji, M., 2017. Void fraction, bubble size and interfacial area measurements in co-current downflow bubble column reactor with microbubble dispersion. Chemical Engineering Science 168, 403–413. https://doi.org/10.1016/j.ces.2017.05.006

Hoffman, P.D., 1992. Mixing in a large storage tank, in: AIChE Symposium Series. American Institute of Chemical Engineers, p. 77.

Hosseinzadeh, M., Ghaemi, A., Shirvani, M., 2017. Hydrodynamic performance evaluation of a novel eductor liquid-liquid extractor using CFD modeling. Chemical Engineering Research and Design 126, 19–31. https://doi.org/10.1016/j.cherd.2017.08.006

Hosseinzadeh, M., Shirvani, M., Ghaemi, A., 2018. A study on mean drop size and drop size distribution in an eductor liquid-liquid extractor. Separation and Purification Technology 201, 205–213. https://doi.org/10.1016/j.seppur.2018.03.020

Hu, J., Wu, W., Wu, M., Yuan, S., 2014. Numerical investigation of the air-oil two-phase flow inside an oil-jet lubricated ball bearing. International Journal of Heat and Mass Transfer 68, 85–93. https://doi.org/10.1016/j.ijheatmasstransfer.2013.09.013

Hu, Y., Liu, Z., Yang, J., Jin, Y., Cheng, Y., 2009. Millisecond mixing of liquids using a novel jet nozzle. Chemical Engineering Science 64, 812–820. https://doi.org/10.1016/j.ces.2008.10.023

Huang, Z., Wang, H., Shuai, Y., Guo, T., Lungu, M., Yang, Yao, Wang, J., Yang, Yongrong, 2018. Hydrodynamics in a jet bubbling reactor: Experimental research and mathematical modeling. AIChE Journal 64, 1814–1827. https://doi.org/10.1002/aic.16041

Ikeda, H., Suzuki, A., 1991. Axial mixing for both dispersed and continuous phases in pulsed perforated-plate extraction column by tracer co-injection method. Journal of Nuclear Science and Technology 28, 426–432. https://doi.org/10.1080/18811248.1991.9731378

Iliuta, I., Thyrion, F.C., Muntean, O., 1998. Axial dispersion of liquid in gas-liquid cocurrent downflow and upflow fixed-bed reactors with porous particles. Chemical Engineering Research and Design 76, 64–72. https://doi.org/10.1205/026387698524488

Jamshidi, A.M., Sohrabi, M., Vahabzadeh, F., Bonakdarpour, B., 2001. Hydrodynamic and mass transfer characterization of a down flow jet loop bioreactor. Biochemical Engineering Journal 8, 241–250. https://doi.org/10.1016/S1369-703X(01)00115-2

Jiménez, S., Andreozzi, M., Micó, M.M., Álvarez, M.G., Contreras, S., 2019. Produced water treatment by advanced oxidation processes. Science of the Total Environment 666, 12–21. https://doi.org/10.1016/j.scitotenv.2019.02.128

Karam, H.J., Billinger, J.C., 1960. Deformation and breakup of liquid droplets in a simple shear field. Industrial & Engineering Chemistry Research 7, 576–581. https://doi.org/10.1021/i160028a009

Kawase, Y., Moo-Young, M., 1986. Liquid phase mixing in bubble columns with Newtonian and non-Newtonian fluids. Chemical Engineering Science 41, 1969–1977. https://doi.org/10.1016/0009-2509(86)87113-5

Khalil, A., Puel, F., Chevalier, Y., Galvan, J.-M., Rivoire, A., Klein, J.-P., 2010. Study of droplet size distribution during an emulsification process using in situ video probe coupled with an automatic image analysis. Chemical Engineering Journal 165, 946–957. https://doi.org/10.1016/j.cej.2010.10.031

Khooshechin, S., Safdari, J., Moosavian, M.A., Mallah, M.H., 2013. Prediction of pressure

drop in liquid-liquid pulsed packed extraction countercurrent columns. International Journal of Heat and Fluid Flow 44, 684–691. https://doi.org/10.1016/j.ijheatfluidflow.2013.09.009

Kirchner, W.G., 1974. Gas entrainment by plunging liquid jets, in: Proceedings of 5 Th Australasian Conference on Hydraulics and Fluid Mechanics. pp. 9–13.

Kitamura, Y., Mishima, H., Takahashi, T., 1982. Stability of jets in liquid-liquid systems. The Canadian Journal of Chemical Engineering 60, 723–731. https://doi.org/10.1002/cjce.5450600602

Kramer, M., Wieprecht, S., Terheiden, K., 2016. Penetration depth of plunging liquid jets - A data driven modelling approach. Experimental Thermal and Fluid Science 76, 109–117. https://doi.org/10.1016/j.expthermflusci.2016.03.007

Kumar, A., Hartland, S., 1999. Computational strategies for sizing liquid-liquid extractors. Industrial & Engineering Chemistry Research 38, 1040–1056. https://doi.org/10.1021/ie9804551

Kumar, A., Hartland, S., 1996. Unified correlations for the prediction of drop size in liquid-liquid extraction columns. Industrial & Engineering Chemistry Research 35, 2682–2695. https://doi.org/10.1021/ie950674w

Kumar, M., Ranjan, S., Tiwari, N.K., 2018. Oxygen transfer study and modeling of plunging hollow jets. Applied Water Science 8, 121. https://doi.org/org/10.1007/s13201-018-0740-8

Lade, V.G., Pakhare, A.D., Rathod, V.K., 2014. Mass transfer studies in pulsed sieve plate extraction column for the removal of tributyl phosphate from aqueous nitric acid. Industrial & Engineering Chemistry Research 53, 4812–4820.

https://doi.org/10.1021/ie401384j

Lau, R., Cui, Z., Fan, L.-S., 2005. Liquid entrainment in high-pressure bubble columns. Industrial & Engineering Chemistry Research 44, 3776–3782. https://doi.org/org/10.1021/ie0491847

Legendre, D., Zenit, R., Velez-Cordero, J.R., 2012. On the deformation of gas bubbles in liquids. Physics of Fluids 24, 043303. https://doi.org/10.1063/1.4705527

Levenspiel, O., 1999. Chemical reaction engineering, Third. ed. John Wiley & Sons.

Li, H., Liu, Z., Chen, J., Sun, B., Guo, Y., He, H., 2017. Correlation of aspect ratio and drag coefficient for hydrate-film-covered methane bubbles in water. Experimental Thermal and Fluid Science 88, 554–565. https://doi.org/10.1016/j.expthermflusci.2017.07.009

Li, M., Wilkinson, D., Patchigolla, K., 2005. Comparison of particle size distributions measured using different techniques. Particulate Science and Technology 23, 265–284. https://doi.org/10.1080/02726350590955912

Lin, T.J., Donnelly, H.G., 1966. Gas bubble entrainment by plunging laminar liquid jets. AIChE Journal 12, 563–571. https://doi.org/10.1002/aic.690120331

Liu, L., Yan, H., Zhao, G., Zhuang, J., 2016. Experimental studies on the terminal velocity of air bubbles in water and glycerol aqueous solution. Experimental Thermal and Fluid Science 78, 254–265. https://doi.org/10.1016/j.expthermflusci.2016.06.011

Liu, L., Zhang, H., Yan, H., Ziegenhein, T., Hessenkemper, H., Zhou, P., Lucas, D., 2021. Experimental studies on bubble aspect ratio and corresponding correlations under bubble swarm condition. Chemical Engineering Science 236, 116551. https://doi.org/10.1016/j.ces.2021.116551

Liu, M., Zhang, T., Wang, T., Yu, W., Wang, J., 2008. Experimental study and modeling on

liquid dispersion in external-loop airlift slurry reactors. Chemical Engineering Journal 139, 523–531. https://doi.org/10.1016/j.cej.2007.08.027

Maaß, S., Paul, N., Kraume, M., 2012. Influence of the dispersed phase fraction on experimental and predicted drop size distributions in breakage dominated stirred systems. Chemical Engineering Science 76, 140–153. https://doi.org/10.1016/j.ces.2012.03.050

Maaß, S., Wollny, S., Voigt, A., Kraume, M., 2011. Experimental comparison of measurement techniques for drop size distributions in liquid/liquid dispersions. Experiments in Fluids 50, 259–269. https://doi.org/10.1007/s00348-010-0918-9

Majumder, S.K., 2019. Hydrodynamics and mass transfer in downflow slurry bubble columns. Apple Academic Press.

Majumder, S.K., 2016. Hydrodynamics and transport processes of inverse bubbly flow. Elsevier.

Mandal, A., 2010. Characterization of gas-liquid parameters in a down-flow jet loop bubble column. Brazilian Journal of Chemical Engineering 27, 253–264. https://doi.org/10.1590/S0104-66322010000200004

Mandal, A., Kundu, G., Mukherjee, D., 2003. Gas holdup and entrainment characteristics in a modified downflow bubble column with Newtonian and non-Newtonian liquid. Chemical Engineering and Processing: Process Intensification 42, 777–787. https://doi.org/10.1016/S0255-2701(02)00134-4

McKeogh, E.J., Ervine, D.A., 1981. Air entrainment rate and diffusion pattern of plunging liquid jets. Chemical Engineering Science 36, 1161–1172. https://doi.org/org/10.1016/0009-2509(81)85064-6

Miwa, S., Moribe, T., Tsutstumi, K., Hibiki, T., 2018. Experimental investigation of air

entrainment by vertical plunging liquid jet. Chemical Engineering Science 181, 251–263. https://doi.org/10.1016/j.ces.2018.01.037

Mlynek, Y., Resnick, W., 1972. Drop sizes in an agitated liquid-liquid system. AIChE Journal 18, 122–127. https://doi.org/10.1002/aic.690180122

Moeller, W.G., Dealy, J.M., 1970. Backmixing in a confined jet. The Canadian Journal of Chemical Engineering 48, 356–361. https://doi.org/10.1002/cjce.5450480403

Morales, C., Elman, H., Pérez, A., 2007. Modeling and simulation of a liquid extraction column with structured packing. Computers & Chemical Engineering 31, 1694–1701. https://doi.org/10.1016/j.compchemeng.2007.02.005

Moreira, É., Pimenta, L.M., Carneiro, L.L., Faria, R.C.L., Mansur, M.B., Ribeiro, C.P., 2005. Hydrodynamic behavior of a rotating disc contractor under low agitation conditions. Chemical Engineering Communications 192, 1017–1035. https://doi.org/10.1080/009864490522542

Myint, W., Hosokawa, S., Tomiyama, A., 2007. Shapes of single drops rising through stagnant liquids. Journal of Fluid Science and Technology 2, 184–195. https://doi.org/10.1299/jfst.2.184

Nosratinia, F., Omidkhah, M.R., Bastani, D., Saifkordi, A.A., 2010. Investigation of mass transfer coefficient under jetting conditions in a liquid-liquid extraction system. Iran Journal of Chemical Engineering 29, 1–12. https://doi.org/10.30492/IJCCE.2010.6713

Ogawa, S., Kobayashi, M., Tone, S., Otake, T., 1982. Liquid phase mixing in the gas-liquid jet reactor with liquid jet ejector. Journal of Chemical Engineering of Japan 15, 469–474. https://doi.org/10.1252/jcej.15.469

Ohkawa, A., Kawai, Y., Kusabiraki, D., Sakai, N., Endoh, K., 1987a. Bubble size, interfacial

area and volumetric liquid-phase mass transfer coefficient in downflow bubble columns with gas entrainment by A liquid jet. Journal of Chemical Engineering of Japan 20, 99–101. https://doi.org/10.1252/jcej.20.99

Ohkawa, A., Kusabiraki, D., Sakai, N., 1987b. Effect of nozzle length on gas entrainment characteristics of vertical liquid jet. Journal of Chemical Engineering of Japan 20, 295–300. https://doi.org/10.1252/jcej.20.295

Okawa, T., Tanaka, T., Kataoka, I., Mori, M., 2003. Temperature effect on single bubble rise characteristics in stagnant distilled water. International Journal of Heat and Mass Transfer 46, 903–913. https://doi.org/10.1016/S0017-9310(02)00345-9

Oliveira, N.S., Silva, D.M., Gondim, M.P.C., Mansur, M.B., 2008. A Study of the drop size distributions and hold-up in short Kühni columns. Brazilian Journal of Chemical Engineering 25, 729–741. https://doi.org/10.1590/S0104-66322008000400010

Park, H.S., Kazachkov, I. V., Sehgal, B.R., 2001. Analysis of plunging jet penetration into liquid pool in isothermal conditions, in: Fourth International Conference on Multiphase Flow, ICMF-2001, May 27 ~ June 1, 2001. New Orleans, Louisiana, U.S.A.

Parmar, H., Pareek, V., Phan, C.M., Evans, G.M., 2015. Influence of jet-jet interaction on droplet size and jet instability in immiscible liquid-liquid system. Chemical Engineering Science 123, 247–254. https://doi.org/10.1016/j.ces.2014.11.015

Parvareh, A., Rahimi, M., Yarmohammadi, M., Alsairafi, A.A., 2009. Experimental and CFD study on the effect of jet position on reactant dispersion performance. International Communications in Heat and Mass Transfer 36, 1096–1102. https://doi.org/10.1016/j.icheatmasstransfer.2009.08.007

Patwardhan, A.W., Gaikwad, S.G., 2003. Mixing in tanks agitated by jets. Chemical

Engineering Research and Design 81, 211–220. https://doi.org/10.1205/026387603762878674

Piwowarek, K., Lipińska, E., Hać-Szymańczuk, E., Pobiega, K., 2021. Propionic acid production from apple pomace in bioreactor using Propionibacterium freudenreichii: an economic analysis of the process. 3 Biotech 11, 1–15. https://doi.org/10.1007/s13205-020-02582-x

Poling, B.E., Prausnitz, J.M., O'connell, J.P., 2001. The properties of gases and liquids. Mcgraw-hill New York.

Prakash, R., Majumder, S.K., Singh, A., 2020. Bubble size distribution and specific bubble interfacial area in two-phase microstructured dense bubbling bed. Chemical Engineering Research and Design 156, 108–130. https://doi.org/10.1016/j.cherd.2020.01.032

Prakash, R., Majumder, S.K., Singh, A., 2019. Particle-laden bubble size and its distribution in microstructured bubbling bed in the presence and absence of a surface active agent. Industrial & Engineering Chemistry Research 58, 3499–3522. https://doi.org/10.1021/acs.iecr.8b05625

Prakash, R., Majumder, S.K., Singh, A., 2018. Flotation technique: Its mechanisms and design parameters. Chemical Engineering and Processing: Process Intensification 127, 249–270. https://doi.org/org/10.1016/j.cep.2018.03.029

Prończuk, M., Bizon, K., 2019. Investigation of the liquid mixing characteristic of an external-loop hybrid fluidized-bed airlift reactor. Chemical Engineering Science 210, 115231. https://doi.org/10.1016/j.ces.2019.115231

Rahimi, M., Parvareh, A., 2005. Experimental and CFD investigation on mixing by a jet in a semi-industrial stirred tank. Chemical Engineering Journal 115, 85–92.

https://doi.org/10.1016/j.cej.2005.09.021

Rajaratnam, N., 1976. Turbulent jets, First. ed, New York, Elsevier Scientific Publishing Company. Elsevier Scientific Publishing Company, New York.

Raymond, F., Rosant, J.-M., 2000. A numerical and experimental study of the terminal velocity and shape of bubbles in viscous liquids. Chemical Engineering Science 55, 943–955. https://doi.org/10.1016/S0009-2509(99)00385-1

Ritter, J., Kraume, M., 2000. On-line measurement technique for drop size distributions in liquid/liquid systems at high dispersed phase fractions. Chemical Engineering & Technology 23, 579–581. https://doi.org/10.1002/1521-4125(200007)23:7<579::AID-CEAT579>3.0.CO;2-Y

Roy, A.K., Kumar, K., 2018. Experimental studies on hydrodynamic characteristics using an oblique plunging liquid jet. Physics of Fluids 30, 122107. https://doi.org/10.1063/1.5058123

Rubio, F.C., Mirón, A.S., García, M.C.C., Camacho, F.G., Grima, E.M., Chisti, Y., 2004. Mixing in bubble columns: a new approach for characterizing dispersion coefficients. Chemical Engineering Science 59, 4369–4376. https://doi.org/10.1016/j.ces.2004.06.037

Ruiz, M.C., Lermanda, P., Padilla, R., 2002. Drop size distribution in a batch mixer under breakage conditions. Hydrometallurgy 63, 65–74. https://doi.org/10.1016/S0304-386X(01)00223-7

Saha, B., Chopade, S.P., Mahajani, S.M., 2000. Recovery of dilute acetic acid through esterification in a reactive distillation column. Catalysis Today 60, 147–157. https://doi.org/10.1016/S0920-5861(00)00326-6

Saien, J., Moradi, V., 2012. Low interfacial tension liquid-liquid extraction with impinging-

jets contacting method: Influencing parameters and relationship. Journal of Industrial and Engineering Chemistry 18, 1293–1300. https://doi.org/10.1016/j.jiec.2012.01.027

Saien, J., Zonouzian, S.A.E., Dehkordi, A.M., 2006. Investigation of a two impinging-jets contacting device for liquid-liquid extraction processes. Chemical Engineering Science 61, 3942–3950. https://doi.org/10.1016/j.ces.2006.01.034

Saito, M., 1988. Experimental study on penetration behaviors of water jet into freon-11 and liquid nitrogen, in: ANS-Proc. 25th Natl. Heat Transfer Conf. pp. 173–183. https://doi.org/https://jopss.jaea.go.jp/search/servlet/search?4032827&language=1.

Samdavid, S., Renganathan, T., Krishnaiah, K., 2016. Hydrodynamics of a cocurrent downward liquid-liquid extraction column. RSC Advances 6, 12439–12445. https://doi.org/10.1039/c5ra23649e

Sangtam, B.T., Majumder, S.K., 2020. Entrainment characteristic of liquid-liquid dispersion in a jet-driven mixing column: Substantial for process intensification in liquid-liquid extraction. Chemical Engineering and Processing: Process Intensification 153, 107927. https://doi.org/10.1016/j.cep.2020.107927

Sangtam, B.T., Prakash, R., Majumder, S.K., 2021a. Mixing characteristics of a liquid-liquid dispersion in a jet-driven mixing column: Developed for the separation of organic pollutants. Industrial & Engineering Chemistry Research. https://doi.org/10.1021/acs.iecr.1c03733

Sangtam, B.T., Prakash, R., Majumder, S.K., 2021b. Drop sizes and its distribution in jet-driven liquid-liquid mixing column: Substantial application for the liquid-liquid extraction process. Chemical Engineering Research and Design 172, 186–203. https://doi.org/10.1016/j.cherd.2021.02.029

Santiago, D.M., Trambouze, P., 1971. Réacteurs parfaitement agitesàdeux phases liquides: mesure de l'aire interfaciale par méthode chimique. Chemical Engineering Science 26, 29–38. https://doi.org/10.1016/0009-2509(71)86078-5

Sarsten, J.A., 1972. Pipeline and Gas J.

Schimetzek, R., Steiff, A., Weinspach, P.M., Molter, E., 1994. Examination of discontinuous jet mixing for designing emergency cooling systems of chemical reactors, in: Institution of Chemical Engineers Symposium Series. Hemsphere Publishing Corporation, pp. 391–398.

Sechremeli, D., Stampouli, A., Stamatoudis, M., 2006. Comparison of mean drop sizes and drop size distributions in agitated liquid-liquid dispersions produced by disk and open type impellers. Chemical Engineering Journal 117, 117–122. https://doi.org/10.1016/j.cej.2005.12.015

Shadpoor, S., Pirouzi, A., Hamze, H., Mazaheri, D., 2021. Determination of Bodenstein number and axial dispersion of a triangular external loop airlift reactor. Chemical Engineering Research and Design 165, 61–68. https://doi.org/10.1016/j.cherd.2020.10.018

Shah, Y.T., Stiegel, G.J., Sharma, M.M., 1978. Backmixing in gas-liquid reactors. AIChE Journal 24, 369–400. https://doi.org/10.1002/aic.690240302

Siddiqui, S.W., 2014. The effect of oils, low molecular weight emulsifiers and hydrodynamics on oil-in-water emulsification in confined impinging jet mixer. Colloids and Surfaces A: Physicochemical and Engineering Aspects 443, 8–18. https://doi.org/10.1016/j.colsurfa.2013.10.027

Siddiqui, S.W., Zhao, Y., Kukukova, A., Kresta, S.M., 2009. Characteristics of a confined

impinging jet reactor: energy dissipation, homogeneous and heterogeneous reaction products, and effect of unequal flow. Industrial & Engineering Chemistry Research 48, 7945–7958. https://doi.org/10.1021/ie801562y

Sivaiah, M., Parmar, R., Majumder, S.K., 2012. Gas entrainment and holdup characteristics in a modified gas-liquid-solid down flow three-phase contactor. Powder Technology 217, 451–461. https://doi.org/10.1016/j.powtec.2011.10.062

Smoot, L.D., Babb, A.L., 1962. Mass Transfer Studies in a Pulsed Extraction Column. Longitudinal Concentration Profiles. Industrial & Engineering Chemistry Fundamentals 1, 93–103. https://doi.org/10.1021/ie401384j

Soh, W.K., Khoo, B.C., Yuen, W.Y.D., 2005. The entrainment of air by water jet impinging on a free surface. Experiments in Fluids 39, 496–504. https://doi.org/10.1007/s00348-005-0965-9

Song, Z., Williams, C.J., Edyvean, R.G.J., 2004. Treatment of tannery wastewater by chemical coagulation. Desalination 164, 249–259. https://doi.org/10.1016/S0011-9164(04)00193-6

Sugihara, K., Sanada, T., Shirota, M., Watanabe, M., 2007. Behavior of single rising bubbles in superpurified water. Kagaku Kogaku Ronbunshu 33, 402–408. https://doi.org/10.1252/kakoronbunshu.33.402

Suresh, A., Srinivasan, T.G., Vasudeva Rao, P.R., Rajagopalan, C. V, Koganti, S.B., 2005. U/Th Separation by counter-current liquid-liquid extraction with tri-sec butyl phosphate by using an ejector mixer-settler. Separation Science and Technology 39, 2477–2496. https://doi.org/10.1081/SS-120039316

Tadrist, L., Alaoui, E.K.O., Occelli, R., Pantaloni, J., 1991. Experimental study of a liquid jet

flowing into another immiscible liquid “a local analysis of the interface.” Experiments in Fluids 12, 67–75. https://doi.org/10.1007/BF00226567

Tamir, A., 1994. Impinging-stream reactors: fundamentals and applications. Elsevier, Amsterdam, The Netherlands.

Taylor, G.I., 1954. The dispersion of matter in turbulent flow through a pipe. Proceedings of the Royal Society of London. Series A. Mathematical and Physical Sciences 223, 446–468. https://doi.org/10.1098/rspa.1954.0130

Taylor, G.I., 1953. Dispersion of soluble matter in solvent flowing slowly through a tube. Proceedings of the Royal Society of London. Series A. Mathematical and Physical Sciences 219, 186–203. https://doi.org/10.1098/rspa.1953.0139

Temos, J., Pratt, H.R.C., Stevens, G.W., 1996. Mass transfer to freely-moving drops. Chemical Engineering Science 51, 27–36. https://doi.org/10.1016/0009-2509(95)00224-3

Tojo, K., Miyanami, K., 1982. Oxygen transfer in jet mixers. The Chemical Engineering Journal 24, 89–97. https://doi.org/10.1016/0300-9467(82)80054-3

Towell, G.D., Ackerman, G.., 1972. Axial mixing of liquid and gas in larger bubble reactors, in: Proceeding 5th European and 2nd International Symposium Chemical Reaction Engineering B3-1. Elsevier.

Trambouze, P., 2004. Chemical reactors: from design to operation. Institut Français du Pétrole Publications, Paris.

Treybal, R.E., 1980. Mass transfer operations, Third. ed. Tata McGraw-Hill Education India., New York.

Tsaoulidis, D., Angeli, P., 2017. Liquid-liquid dispersions in intensified impinging-jets cells. Chemical Engineering Science 171, 149–159. https://doi.org/10.1016/j.ces.2017.05.016

Tung, L.S., Luecke, R.H., 1986. Mass transfer and drop sizes in pulsed-plate extraction columns. Industrial & Engineering Chemistry Process Design and Development 25, 664–673. https://doi.org/10.1021/i200034a012

Van de Sande, E., Smith, J.M., 1975. Mass transfer from plunging water jets. The Chemical Engineering Journal 10, 225–233. https://doi.org/10.1016/0300-9467(75)88040-3

Van Woezik, B.A.A., Westerterp, K.R., 2000. Measurement of interfacial areas with the chemical method for a system with alternating dispersed phases. Chemical Engineering and Processing: Process Intensification 39, 299–314. https://doi.org/10.1016/S0255-2701(99)00089-6

Velan, M., Ramanujam, T.K., 1994. Influence of reactor geometry on mixing characteristics in a down flow jet loop bioreactor: newtonian and non-newtonian fluids. Bioprocess Engineering 11, 101–106. https://doi.org/10.1007/BF00369605

Voulgaropoulos, V., Jamshidi, R., Mazzei, L., Angeli, P., 2019. Experimental and numerical studies on the flow characteristics and separation properties of dispersed liquid-liquid flows. Physics of Fluids 31, 73304. https://doi.org/10.1063/1.5092720

Wanchoo, R.K., Sharma, S.K., Gupta, R., 2003. Shape of a Newtonian liquid drop moving through an immiscible quiescent non-Newtonian liquid. Chemical Engineering and Processing: Process Intensification 42, 387–393. https://doi.org/10.1016/S0255-2701(02)00059-4

Wang, Y.D., Fei, W.Y., Sun, J.H., Wan, Y.K., 2002. Hydrodynamics and mass transfer performance of a modified rotating disc contactor (MRDC). Chemical Engineering Research and Design 80, 392–400. https://doi.org/10.1205/026387602317446434

Wasewar, K.L., 2006. A design of jet mixed tank. Chemical and Biochemical Engineering

Quarterly 20, 31–46.

Wellek, R.M., Agrawal, A.K., Skelland, A.H.P., 1966. Shape of liquid drops moving in liquid media. AIChE Journal 12, 854–862. https://doi.org/10.1002/aic.690120506

Wódzki, R., Nowaczyk, J., Kujawski, M., 2000. Separation of propionic and acetic acid by pertraction in a multimembrane hybrid system, Separation and Purification Technology. Elsevier. https://doi.org/10.1016/S1383-5866(00)00187-8

Yadav, H., Agrawal, A., Srivastava, A., 2016. Mixing and entrainment characteristics of a pulse jet. International Journal of Heat and Fluid Flow 61, 749–761. https://doi.org/10.1016/j.ijheatfluidflow.2016.08.006

Yang, K., Chu, G., Zou, H., Sun, B., Shao, L., Chen, J.F., 2011. Determination of the effective interfacial area in rotating packed bed. Chemical Engineering Journal 168, 1377–1382. https://doi.org/10.1016/j.cej.2011.01.100

Yerushalmi, L., Alimahmoodi, M., Behzadian, F., Mulligan, C.N., 2013. Mixing characteristics and liquid circulation in a new multi-environment bioreactor. Bioprocess and Biosystems Engineering 36, 1339–1352. https://doi.org/10.1007/s00449-012-0836-8

Zehner, P., 1982. Impuls-, Stoff-und Wärmetransport in Blasensäulen. Chemie Ingenieur Technik 54, 248–251. https://doi.org/10.1002/cite.330540311

Zhang, S.H., Yu, S.C., Zhou, Y.C., Su, Y.F., 1985. A model for liquid-liquid extraction column performance-The influence of drop size distribution on extraction efficiency. The Canadian Journal of Chemical Engineering 63, 212–226. https://doi.org/10.1002/cjce.5450630206

Zhu, Y., Oğuz, H.N., Prosperetti, A., 2000. On the mechanism of air entrainment by liquid jets at a free surface. Journal of Fluid Mechanics 404, 151–177.

https://doi.org/10.1017/S0022112099007090

Ziqi, C., Yuyun, B., Zhengming, G., 2010. Hydrodynamic behavior of a single bubble rising in viscous liquids. Chinese Journal of Chemical Engineering 18, 923–930. https://doi.org/10.1016/S1004-9541(09)60149-X